# Diurnal control of iron responsive element (IRE)-containing mRNAs through iron regular proteins IRP1 and IRP2 is mediated by feeding rhythms

Hima Priyanka Nadimpalli[1,#], Georgia Katsioudi[1,#], Enes S. Arpa[1], Lies Chikhaoui[1], A. Bulak Arpat[1], Angelica Liechti[1], Gaël Palais[2], Claudia Tessmer[3], Ilse Hofmann[3], Bruno Galy[2], David Gatfield[1]*

Affiliations:

[1] Center for Integrative Genomics, University of Lausanne, 1015 Lausanne, Switzerland.

[2] German Cancer Research Center (DKFZ), Division of Virus-associated Carcinogenesis, Im Neuenheimer Feld 280, 69120, Heidelberg, Germany.

[3] German Cancer Research Center (DKFZ), Core Facility Antibodies, Im Neuenheimer Feld 280, 69120, Heidelberg, Germany.

# equal contribution

* Corresponding author

## Abstract

A central mechanism for cellular iron homeostasis involves iron regulatory proteins, IRP1 and IRP2, that interact with iron regulatory elements (IREs) on mRNAs. IRPs act as sensors of metabolic cues (foremost of iron itself) and can regulate either translation or transcript stability, depending on IRE location within the mRNA. In liver, IRP2 is widely considered the principle player mediating IRE regulation. Here, we uncover high-amplitude diurnal rhythms in the regulation of several prominent IRE-containing mRNAs in liver, compatible with maximal IRP activity at the onset of the dark phase of the day (a timepoint likely underrepresented in previous studies on IRP/IRE regulation). We find that IRP2 protein abundance itself oscillates over the day, yet ribosome profiling in livers from IRP2-deficient mice uncovers that IRP2 is dispensable for maximal repression of its rhythmically regulated target mRNAs at the time of its highest abundance, i.e. the light-dark transition. These findings are compatible with temporally controlled redundancy in IRP activities, with IRP2 exclusively mediating regulation of IRE-containing transcripts in the light phase and redundancy, conceivably with IRP1, at dark onset. We further unveil that the identified diurnal IRP/IRE regulation can ensue in the absence of a functional circadian clock as long as feeding is rhythmic, and that it follows feeding rhythms also in the presence of a clock, thus identifying feeding-associated signals as the dominant driver of IRP/IRE rhythmicity. Altogether, our study identifies a novel level of regulatory control and complexity in a metabolic pathway that had been considered well-understood since a long time.

## Introduction

Mammalian behaviour, physiology and metabolism undergo distinct changes over the course of the day (reviewed in [1]). These rhythmic patterns are orchestrated to large extent via the body's internal timekeeping system, the circadian clock. Molecular circadian oscillators can be found in virtually all cell types of the body and are hierarchically organised. The master clock in the brain's suprachiasmatic nuclei (SCN) is entrained to the environmental light-dark cycle through signals that it receives via projections from the retina. In turn, the SCN entrains (via e.g. hormones, body temperature cycles, feeding-fasting cycles) the peripheral oscillators that are active in the remainder of the organism. Across cell types, the rhythm-generating core clock has a similar molecular makeup that is based on negative transcriptional feedback loops in gene expression (reviewed in [2]). In the main loop, the negative feedback involves the transcriptional activators BMAL1:CLOCK (and/or BMAL1:NPAS2 in some neurons) that drive the rhythmic expression of the PERIOD and CRYPTOCHROME proteins which act as repressors of BMAL1:CLOCK-mediated transcription. Downstream of the core clock mechanism, BMAL1:CLOCK and other rhythmic transcriptional activities drive daily cycles in gene expression at hundreds to thousands of loci known as clock-controlled genes (CCGs). The resulting transcriptome-scale oscillations in mRNA abundance have been extensively studied across a variety of organs and cell types, genetic mouse models, light-dark regimens, metabolic conditions and dietary treatments. Notably, metabolism is a key rhythmically regulated process in organs such as the liver, with many links to human disease [3].

While rhythmic transcription is thought to be the principal driver of oscillating gene expression, various roles for post-transcriptional mechanisms have emerged as well (reviewed in [4, 5]). Conceptually, mRNA accumulation can be rendered rhythmic by time-of-day-dependent modulation of its stability, rather than of its transcription; and proteins can display daily changes in abundance in the absence of rhythmic mRNA, due to time-of-day-dependent control of translation and/or protein stability. To this end, previous studies using ribosome profiling (ribo-seq) in mouse liver around-the-clock have identified transcripts and pathways that are rhythmically regulated specifically at the level of translation, uncovering ribosomal protein and translation factor biosynthesis as the most prominent group of proteins regulated by this mechanism [6, 7].

An intriguing case of rhythmic translation that we noted in a previous study, are three transcripts involved in iron metabolism, *Ferritin light chain 1 (Ftl1), Ferritin heavy chain 1 (Fth1)* and *Aminolevulinic acid synthase 2 (Alas2)* [6]. The observation that Ferritin mRNAs (encoding the main iron storage proteins) are translationally repressed and activated, respectively, in response

71 to low and high iron concentrations, led to the discovery of the translational control element known
72 as the IRE (iron-responsive element) more than 40 years ago [8, 9]; *Alas2*, encoding the enzyme
73 that catalyses the first step in the heme biosynthetic pathway especially in erythrocytes, was
74 identified as IRE-containing a few years later [10] (please note that *Alas2* is distinct in its regulation
75 from *Alas1*, which specifies the housekeeping version of the enzyme and is well-known for its
76 very high transcriptional rhythmicity [11]). Since then, several other IRE-containing transcripts
77 have been identified and validated, and many more predicted ([12] and see below). IREs act
78 together with IRE-binding proteins (IRPs; iron-regulatory proteins) in response to physiological
79 iron availability and other cues ($O_2$, $H_2O_2$, NO) (reviewed in [13, 14]). The liver, which is the major
80 iron storage site in mammals, has been used as a model organ to study IRE/IRP regulation. From
81 the analysis of livers of mice deficient for the known IRPs, IRP1 (encoded by the *Aco1* gene) and
82 IRP2 (encoded by *Ireb2*), it has been concluded that IRP2 is the main actor in hepatic IRE
83 regulation, whereas IRP1 has a limited role, unable to fully replace IRP2 in the regulation of the
84 most prominent IRE-containing transcripts (e.g. [15-17]). Importantly, none of these studies
85 considered a possible time-of-day component in the regulatory mechanism.
86 In the present work, we first explore in a systematic fashion to what extent IRE-containing
87 transcripts beyond *Ftl1, Fth1* and *Alas2* are subject to rhythmic regulation. We then analyse
88 dependency of rhythmic regulation on the two IRPs using ribo-seq in livers collected at defined
89 timepoints in the light vs. dark phase from *Aco1/Irp1* and *Ireb2/Irp2* knockout mice. Finally, we
90 analyse previously published datasets to infer to what extent rhythmic IRE-regulation is a
91 circadian clock- vs. feeding-driven phenomenon. Our findings lead to a re-evaluation of current
92 models of IRP1 vs. IRP2-dependence of hepatic IRE-regulation, a key mechanism in organismal
93 iron homeostasis, and they expand our knowledge of the intricate connections between rhythmic
94 gene expression and metabolism.
95
96 **Results**
97 *A subset of iron response element-containing transcripts is rhythmically translated in mouse liver*
98 In our previous study [6] we used RNA-seq and ribo-seq on mouse liver samples collected around-
99 the-clock to identify and compare daily gene expression rhythms occurring at the level of mRNA
100 abundance and translation (Fig. 1A). These analyses had revealed rhythmicity across various
101 iron homeostatic genes, from cellular iron uptake to intracellular iron transport and storage,
102 hepatic heme and Fe-S cluster biosynthesis, cellular iron export, and systemic hormonal iron
103 homeostasis [6]. Of the almost 20 identified rhythmically regulated iron metabolic genes, the
104 majority showed similar oscillations in both RNA-seq and ribo-seq data, indicating that their

105 oscillations were driven at the level of transcription (and/or RNA stability). However, three
106 transcripts formed a notable exception – *Ftl1, Fth1* and *Alas2* were invariable in their mRNA
107 abundance, yet they showed robust rhythms in ribosome occupancy. All three transcripts contain
108 an IRE in their 5' untranslated region (5' UTR) [12]. Such 5' IREs act in concert with iron regulatory
109 proteins, IRP1 and IRP2, which bind to the IREs and inhibit translation under conditions of low
110 intracellular iron and as a function of other physiological cues (Fig. 1B-C) [12]. IRE sequences
111 fold into specific hairpin structures (Fig. 1D) that are crucial for IRP binding and have been used
112 for IRE predictions [18, 19]. In mammals, more than a dozen IRE-containing mRNAs have been
113 reported, mostly in 5' UTRs. In rare cases, IREs are in the 3' UTR. In *Transferrin receptor (Tfrc*)
114 mRNA, multiple 3' IREs regulate transcript stability in an IRP-dependent manner, involving
115 endonucleolytic cleavage (Fig. 1C) [20]. Single 3' IREs have also been identified in *Slc11a2* (also
116 known as *Dmt1,* for *Divalent metal transporter 1*) [21] and *Profilin 2 (Pfn2)* [22], but their
117 mechanisms of action appear to be distinct from regulation of *Tfrc*.
118 With *Ftl1, Fth1* and *Alas2* translation showing robust oscillations [6], we first wished to investigate
119 whether rhythmic translation was more commonly found across IRE-containing transcripts. To
120 this end, we used our liver [6] and kidney [23] RNA-seq and ribo-seq datasets to compare time-
121 resolved gene expression profiles of additional IRE-containing transcripts. As compared to the
122 robust rhythms in translation seen for *Fth1, Ftl1* and *Alas2* in liver (Fig. 1E, upper), other 5' IRE-
123 containing mRNAs lacked high-amplitude oscillations in ribosome occupancy. Thus, the
124 translation of *Ferroportin* (*Slc40a1)* mRNA showed, at best, low-amplitude oscillations, whereas
125 *Aconitase 2 (Aco2)* and *Hif2a/Endothelial PAS domain-containing protein 1 (Epas1)* were non-
126 rhythmic (Fig. 1F, upper), despite harbouring well-characterized 5' IREs [24-26]. We next
127 compared the time-resolved gene expression profiles from liver to those in kidney (Fig. 1E-F,
128 lower). *Ftl1* and *Fth1* showed blunted rhythmic profiles in kidney, resembling the low amplitudes
129 seen for *Slc40a1* (please note that low expression of *Alas2* in kidney precluded drawing strong
130 conclusions); *Aco2* and *Epas1* were clearly non-rhythmic in kidney at RNA abundance and
131 translational levels. In summary, we concluded that, first, rhythmic translational regulation in liver
132 only occurred on a subset of 5' IRE-containing transcripts. Second, rhythmic translational
133 regulation showed tissue-specificity, with higher amplitudes in liver as compared to kidney.
134 We considered it a plausible hypothesis that distinct features in IRE sequence or structure could
135 underlie the observed differences in regulation. We inspected whether the IRE sequences and
136 secondary structure predictions showed specific characteristics correlating with rhythmic vs. non-
137 rhythmic translation (Fig. 1G-H). Despite individual differences across IREs with regard to the
138 length of the paired stem, the positions of additional bulge nucleotides, or the location of the IRE

139 relative to the 5' end of the mRNA or the translation start codon, we did not identify a particular
140 feature that would distinguish the rhythmicity-associated IREs (Fig. 1G) from the other IREs (Fig.
141 1H).
142
143 *Rhythmic abundance of 3' IRE-containing* Transferrin receptor *mRNA is controlled post-*
144 *transcriptionally and altered in nonsense-mediated mRNA decay mutant livers*
145 Next, we analysed the daily expression profiles of *Tfrc* mRNA, which harbours multiple 3' IREs
146 (Fig. 2A) that regulate transcript stability (Fig. 1C) [20]. *Tfrc* mRNA abundance was robustly
147 rhythmic in both liver and kidney and ribosome footprints closely matched the mRNA profiles,
148 indicating that no additional rhythmicity was imparted at the level of translation (Fig. 2B). We then
149 confirmed that the observed *Tfrc* mRNA rhythms were of post-transcriptional origin, in line with
150 the 3' IRE mechanism and previous observations [6, 27]. To this end, we leveraged two around-
151 the-clock mouse liver datasets [28, 29] in which we had carried out RNA-seq on total RNA,
152 allowing the quantification of both unspliced pre-mRNA (intron-mapping reads) and of mature
153 mRNA (exon-mapping reads). With pre-mRNA levels serving as a proxy for nascent
154 RNA/transcription at the *Tfrc* locus, both datasets confirmed that *Tfrc* was transcribed in a non-
155 rhythmic fashion, yet its mRNA accumulated rhythmically around-the-clock (Fig. 2C-D, data from
156 control mice). We concluded that *Tfrc* rhythms were generated post-transcriptionally by
157 modulating transcript stability in a diurnal fashion. This finding is further supported by a recent
158 preprint [30].
159 One of the analysed wild-type liver datasets (Fig. 2C) was part of a study that contained a
160 matching cohort of animals that were deficient in miRNA biogenesis due to the hepatocyte-
161 specific deletion of *Dicer* [28]. It has previously been proposed that *Tfrc* mRNA stability is
162 regulated by the interplay between IRPs and miR-7/miR-141 binding at the 3' IRE stem-loops
163 [31]. However, because *Tfrc* mRNA profiles were unaltered in *Dicer* knockouts (Fig. 2C), we deem
164 it unlikely that miRNA-mediated mechanisms make strong contributions to hepatic 3' IRE
165 regulation. The other analysed dataset (Fig. 2D) contained a matching cohort of animals that
166 expressed a catalytically inactive, mutant version of the endonuclease SMG6; this enzyme
167 degrades transcripts targeted through the nonsense-mediated decay (NMD) pathway [29].
168 Interestingly, at all timepoints *Tfrc* mRNA abundances were post-transcriptionally increased in
169 *Smg6* mutant livers, leading to >2-fold higher mRNA levels; still, mutants showed similar
170 rhythmicity dynamics and peak-to-trough amplitudes in the range of ca. 3.2-fold (mutants) vs. 2.6-
171 fold (controls) (Fig. 2D). This finding could indicate that SMG6 is implicated, directly or indirectly,
172 in the regulation of *Tfrc* mRNA stability, potentially as a part or independently of the Roquin- and

173 Regnase-1-dependent pathways previously implicated in *Tfrc* mRNA decay [32, 33]. Another
174 possibility is that the *Tfrc* locus produces high levels of unproductively spliced transcript isoforms
175 that are subsequently cleared by NMD; indeed, several *Tfrc* mRNA variants with retained introns
176 are annotated in Ensembl (www.ensembl.org/ - locus ENSMUSG00000022797). To evaluate the
177 impact of NMD on mature TFRC levels, we analysed its protein abundance by Western blot in
178 control and NMD-deficient livers around-the-clock (Fig. 2E, F). TFRC protein abundance in wild-
179 type animals was minimal and maximal at *Zeitgeber* Time (ZT) 12 and 20, respectively, with a 2-
180 fold peak-to-trough amplitude that is consistent with its mRNA rhythmicity (Fig. 2D). In *Smg6*
181 mutant livers, the around-the-clock pattern of TFRC levels was irregular with a 1.8-fold peak-to-
182 trough amplitude, and its average abundance over-the-day was increased 1.4-fold as compared
183 to controls (Fig. 2F). Hence, the effect of NMD loss-of-function on TFRC protein was quantitatively
184 considerably smaller than what could have been expected from the *Tfrc* mRNA increase (Fig.
185 2D). We thus propose that most likely the main role of NMD in *Tfrc* regulation consists in the
186 clearance of unproductive mRNA isoforms, although some effect on regulating mature, translated
187 *Tfrc* mRNA is plausible as well. Altogether, involvement of NMD factors in *Tfrc* mRNA regulation
188 is not unprecedented [34] and remains intriguing, in particular because of recent work that
189 identified TFRC and iron homeostasis as regulators that act *upstream* of NMD, through a
190 mechanism that relies on the Fe-S cluster-containing ribosome recycling factor ABCE1 [35]. One
191 may thus speculate about a possible feedback mechanism, with (i) TFRC protein controlling
192 cellular iron uptake, (ii) intracellular iron availability controlling NMD activity, and (iii) NMD factors
193 implicated in regulating *Tfrc* mRNA stability.
194
195 *Rhythmic translation/mRNA abundance predicts phases of maximal and minimal IRP activity*
196 The above analyses established that high-amplitude rhythmic regulation was particularly
197 prominent for four IRE-containing transcripts in mouse liver. Of these, the three translationally
198 regulated transcripts *(Ftl1, Fth1, Alas2)* showed similar rhythmic phase, with a peak in translation
199 occurring at approximately ZT4-6 and a trough at ~ZT12 (Fig. 1E). Given that the association with
200 IRPs inhibits the translation of IRE-containing transcripts (Fig. 1B-C), we would expect IRP
201 binding/activity on *Ftl1, Fth1* and *Alas2* mRNAs to be minimal at ZT4-6 and maximal at ZT12. For
202 *Tfrc*, the binding of IRPs to the IREs would increase the stability of the mRNA and (assuming
203 constant rates in *Tfrc* mRNA transcription) maximal IRP activity would be predicted during the
204 rising phase of *Tfrc* mRNA abundance, i.e. around ZT12 as well. Therefore, all four rhythmic gene
205 expression events would be consistent with a mechanism involving rhythmic IRP activity on IREs
206 that is minimal and maximal at ZT4-6 and ZT12, respectively (Fig. 2G).

207 The observed diurnal regulation could be mediated simply by daily changes in IRP protein
208 abundance; we had dismissed this mechanism, however, in our previous study in which we had
209 observed no rhythmicity (or, at most, very modest daily changes) for liver IRP1/ACO1 or
210 IRP2/IREB2 at the level of mRNA, ribosome footprints or protein [6]. Since publication of our
211 study, however, it has been reported that the antibody we had used to quantify IRP2/IREB2
212 (abcam ab1811539) not only detects IRP2/IREB2 (as marketed by the vendor at the time), but
213 also IRP1/ACO1 [36]. Therefore, our original analysis of around-the-clock IRP2 protein levels was
214 undoubtedly flawed, representing an overlay of both IRPs rather than IRP2 specifically. Moreover,
215 it has been reported that in colon cancer cells, the *Ireb2* gene is circadianly transcribed through
216 BMAL1:CLOCK, engendering *Ireb2* mRNA and IRP2/IREB2 protein oscillations that subsequently
217 regulate *Tfrc* stability in a rhythmic fashion [37]. The ensemble of these findings prompted us to
218 revisit the temporal dynamics of IRP expression across our datasets. Thus, our RNA-seq and
219 ribo-seq data showed modest rhythmicity (<1.5-fold peak-to-trough amplitudes) for *Aco1* and
220 *Ireb2* in liver but not in kidney (Fig. 2H). For *Ireb2*, the mRNA phase – maximal abundance around
221 ZT10 – was indeed compatible with the BMAL1:CLOCK regulation that has been reported from
222 colon cancer cells [37]. However, the shallow peak-trough amplitudes that *Ireb2* displays for both
223 RNA and pre-mRNA (Fig. 2I, lower) indicated that rhythmic transcriptional activation through
224 BMAL1:CLOCK would not appear to be an important driver of *Ireb2* mRNA synthesis in liver. For
225 comparison, in the same dataset *Arntl/Bmal1* itself, and well-established BMAL1:CLOCK targets
226 such as *Dbp* [38], present very high amplitude mRNA and pre-mRNA oscillations (Fig. 2J).
227 The main regulation of IRP1 activity and of IRP2 abundance occurs through post-translational
228 mechanisms (Fig. 1B) [14]. Given the issues with antibody specificity described above, we re-
229 evaluated IRP1 and IRP2 protein levels around-the-clock using highly specific monoclonal
230 antibodies that are free of cross-reactivity (see later, Fig. 4G, J). Using the same time series of
231 pooled liver protein extracts as for TFRC quantification (Fig. 2E), no high-amplitude rhythmicity
232 was apparent for ACO1/IRP1 (Fig. 2K, L). By contrast, the Western blot for IREB2/IRP2 revealed
233 high-amplitude rhythmic protein accumulation in the control animals (*Smg6*$^{wt/wt}$), with minimal and
234 maximal protein abundances around ZT4 and ZT12, respectively (Fig. 2N, O). In the matching
235 time series from *Smg6*$^{mut/mut}$ animals, the IRP2 rhythm was blunted (Fig. 2N, O). The difference
236 in IRP2 protein levels quantified from single liver samples (ZT4 and ZT12; control animals)
237 showed a ca. 10-fold amplitude with some inter-individual variability (Fig. 2M, P). Next, we
238 analysed the levels of FBXL5, which is the F-box protein that targets IREB2/IRP2 for proteasomal
239 degradation and is key for the regulation of IRP2 stability and abundance; according to the
240 established mechanism, FBXL5 acts as an iron sensor that is stabilized by Fe binding under high

241 iron conditions, yet unfolded and degraded during iron scarcity [39, 40]. In addition, an FBXL5-
242 independent mechanism of IREB2/IRP2-dependent target regulation has recently been identified
243 as well [41]. However, our western blot analysis in the control liver time series and in single liver
244 samples indicated that FBXL5 protein levels did not show the same marked rhythmicity as
245 displayed by IREB2/IRP2 (Fig. 2Q-S). Thus, we deem it unlikely that the observed changes in
246 IREB2/IRP2 (Fig. 2N, O) are a direct outcome of FBXL5 availability. Interestingly, *Smg6*$^{mut/mut}$
247 animals displayed blunted IRP2 rhythmicity compared to wild-type (Fig. 2N, O). This suggests
248 that the NMD pathway may somehow contribute to daily changes in IRP2 abundance in liver,
249 which together with recent report of FBXL5-independent mechanism of IREB2/IRP2-dependent
250 target regulation [41], highlights the complexity of IRP2 regulation.
251
252 In vivo *recording of diurnal gene expression oscillations shows unperturbed circadian*
253 *mPER2::LUC reporter rhythms in* Aco1 *and* Ireb2 *knockout mice*
254 We concluded from the above analyses that rhythmicity of the IRE-containing transcripts *Ftl1,*
255 *Fth1, Alas2* and *Tfrc* was compatible with diurnal regulation through IRPs, with a trough and peak
256 of IRP activity in the early light phase and at the light-dark transition, respectively. Conceivably,
257 the mechanism underlying these daily changes could be related to oscillations in IREB2/IRP2
258 levels that followed a similar rhythm (at least in the control animal time series) with lower IRP2 in
259 the light phase and higher IRP2 in the dark phase (Fig. 2N, O). In support of this hypothesis,
260 impact on IRE regulation has been reported mainly upon IRP2 deficiency and not so upon IRP1
261 loss [15, 42]. Yet, IRP1 has in the past been suggested to be particularly abundant in liver, and
262 our ribosome footprint data confirmed that ACO1/IRP1 is more highly expressed than
263 IREB2/IRP2, with a translational output for ACO1/IRP1 >5-fold higher than that of IREB2/IRP2
264 (Fig. 2H; compare maximal liver footprint Reads Per Kilobase per Million mapped reads of ca.
265 150 for *Aco1* and of ca. 25 for *Ireb2*). Importantly, previous studies have not addressed the
266 possibility of temporal control of IRP1-mediated IRE regulation in liver. Hence, depending on the
267 affinities that IRP1 and IRP2 have for individual IREs, and on additional regulatory mechanisms
268 that may be in place, either of the IRPs, or both, may contribute to rhythmic regulation, even if
269 only IREB2/IRP2 appears to undergo daily changes in protein abundance.
270 We set out to determine experimentally how rhythmic target regulation would be changed in the
271 absence of IRP1 or IRP2. To this end, we made use of constitutive *Aco1* and *Ireb2* knockout
272 mouse strains [43]. These knockout mice present with systemic alterations to iron homeostasis
273 and phenotypic abnormalities, including in liver (reviewed in [44]); moreover, there are
274 documented links between iron and the circadian timekeeping mechanism itself. For example,

275 several core clock proteins contain heme [11, 45, 46] and the transcription of *Per1* and *Per2* has
276 been reported as sensitive to iron accumulation through a mechanism that involves histone
277 methylation state [47]. Therefore, we first explored whether whole-body *Aco1* or *Ireb2* knockout
278 engendered phenotypes in entrained liver clock rhythms that could potentially confound the
279 specific analysis of rhythmic IRP/IRE regulation. We used a method for the real-time recording of
280 liver gene expression in freely moving mice [48, 49] that relies on luciferase reporters, luciferin
281 delivery via an osmotic minipump, and highly sensitive bioluminescence photon counting (Fig.
282 3A). Into the *Aco1* and *Ireb2* knockout lines, we crossed the *mPer2::luc* knock-in allele [50] that
283 expresses a protein fusion between core clock component PER2 and firefly luciferase, serving as
284 a precise readout of diurnal oscillations. We carried out real-time recordings of liver rhythms under
285 conditions that ensured light-entrainment of the master (SCN) clock to an external 24-hour light-
286 dark cycle by means of a skeleton photoperiod, i.e. two 30 min light pulses applied at times
287 corresponding to the beginning and to the end of the light phase in a 12h-light-12h-dark (LD12:12)
288 cycle (Fig. 3B). Our experiments revealed rhythmic bioluminescence rhythms in wild-type
289 animals, as expected, and also in littermate animals that were knockouts for either of the IRPs
290 (Fig. 3C-F). For *Aco1*$^{-/-}$ mice, the phase of entrained mPER2::LUC reporter oscillations was
291 virtually indistinguishable from controls (Fig. 3D). In the *Ireb2*$^{-/-}$ animals, the entrained
292 mPER2::LUC phase was minimally delayed (~0.5 h) as compared to controls (Fig. 3F), yet no
293 other overt differences were apparent. We nevertheless verified that the liver clock in *Ireb2*
294 knockouts was fully functional by recording free-running rhythms from liver organ explants (Fig.
295 3G). Free-running bioluminescence rhythms from *Ireb2* knockouts and controls (Fig. 3H) and their
296 quantification (Fig. 3I) indicated overall comparable oscillations *ex vivo*, yet with higher variability
297 in period length between individual explants in the knockouts. Altogether, our data suggested that
298 diurnal oscillations in liver were comparable between IRP knockouts and their respective controls,
299 and in particular that entrained clock phases between genotypes showed good correspondence.
300

301 *Timepoint-specific gene expression datasets from IRP-deficient livers allow analysis of diurnal*
302 *regulation*

303 For our further analyses we selected the two timepoints when rhythmic IRP/IRE activity would be
304 low (ZT5) and high (ZT12), respectively, leading to high and low translation efficiency *(Ftl1, Fth1,*
305 *Alas2)* and mRNA turnover *(Tfrc)* (Fig. 4A). We reasoned that in the simplest scenario, one of the
306 IRPs (e.g. IRP2, the most potent IRE-regulator in liver according to the literature) was singly
307 responsible for rhythmic target regulation. This rhythm would then be detectable in the control
308 livers when comparing the two timepoints, yet absent in the livers from animals deficient for the

309 rhythm-relevant IRP. More complex regulatory scenarios are conceivable, too, such as redundant
310 regulation by the two IRPs, which would lead to no, or partial deregulation of rhythmicity in the
311 knockouts. We collected 3 livers per timepoint and genotype (*Aco1*$^{-/-}$ and *Ireb2*$^{-/-}$; plus their
312 respective, matched *Aco1*$^{+/+}$ and *Ireb2*$^{+/+}$ controls carrying the same genetic background) and
313 prepared RNA-seq and ribo-seq libraries (Fig. 4B). After sequencing and analysis, quantification
314 of *Aco1*-mapping ribosome protected fragments (RPFs) in *Aco1*$^{-/-}$ livers confirmed the knockout
315 at the level of ACO1/IRP1 translation/protein biosynthesis (Fig. 4C, top panel). Because in the
316 knockout allele the open reading frame is disrupted yet still produces an mRNA from the locus
317 [43], the reduction in *Aco1* in the RNA-seq data was less pronounced (Fig. 4C, middle panel).
318 *Aco1* translation efficiency (TE; defined as RPF/RNA ratio) was decreased in the knockouts as
319 expected (Fig. 4C, lower panel). In livers from *Ireb2*-deficient animals, *Aco1* RNA and RPFs were
320 decreased by 10-20% as compared to their littermate controls (Fig. 4D), indicating that
321 IREB2/IRP2 loss did not lead to compensatory higher IRP1 biosynthesis. Overall analogous
322 observations were made for *Ireb2* expression, which showed the expected decrease in the *Ireb2*$^{-}$
323 $^{/-}$ animals at RPF and TE level (Fig. 4F, upper and lower panels), but not for the RNA (Fig. 4F,
324 middle panel). In *Aco1* knockouts, *Ireb2* expression was largely unchanged at the RPF level,
325 indicating that there was no substantial compensatory upregulation (Fig. 4E). We next validated
326 knockout and possible compensatory effects by Western blot. These analyses confirmed the
327 expected loss of ACO1/IRP1 in *Aco1*$^{-/-}$ mice (Fig. 4G, H). In these animals, IREB2/IRP2
328 abundance showed a tendency towards increased levels that did not reach statistical significance
329 (Fig. 4G, I). Higher abundance of IREB2/IRP2 at ZT12 vs. ZT5 was evident as well, although
330 quantitively less pronounced than in the around-the-clock time series analysed before (compare
331 Fig. 4G, I with Fig. 2M-P). In the *Ireb2* cohort, knockouts were devoid of IREB2/IRP2 protein as
332 expected (Fig. 4J, L). In the control animals from this cohort, IREB2/IRP2 increased in abundance
333 from ZT5 to ZT12 in a quantitatively minor (yet statistically significant) fashion (Fig. 4L). In
334 summary, we concluded that the datasets obtained from the two timepoints and genotypes would
335 allow the analysis of interactions between IRP function and time-of-day and, more specifically, to
336 investigate whether the identified rhythmic regulation could be attributed specifically to one of the
337 IRPs. Moreover, our experiments validated the specificity of the IRP1 and IRP2 antibodies.
338 Finally, although we observed a significant difference in IRP2 abundance between light-phase
339 and dark-phase timepoints across different independent datasets, the fold-changes seen in the
340 three cohorts (Fig. 2O, P; Fig. 4I, L) were highly variable, pointing towards limited robustness of
341 IRP2 rhythmicity.
342

343 *Previous observations on IRE-IRP regulation were likely biased towards mechanisms occurring*
344 *during the light phase of the day*
345 A number of previous studies have quantified how the expression of IRE-containing transcripts is
346 altered in IRP knockout livers (e.g. [15-17, 43]). These studies focused in particular on Ferritin
347 protein levels and on *Tfrc* mRNA abundance as readouts in IRP1- or IRP2-deficient mice. A main
348 outcome from these studies was that the targeted deletion of *Ireb2/Irp2*, but not of *Aco1/Irp1*, is
349 associated with increased hepatic Ferritin protein and reduced *Tfrc* mRNA levels. These findings
350 led to the model that IREB2/IRP2 is the main actor in hepatic IRE regulation and that ACO1/IRP1
351 cannot compensate for its loss. None of these studies, however, used ribo-seq to specifically
352 quantify translation rates, nor did they consider a possible temporal component in regulation. As
353 the timing of animal sacrifice is not reported in previous publications on hepatic IRE regulation,
354 we estimated a likely time window during which liver sampling could have been carried out.
355 Standard animal housing usually follows an LD12:12 schedule that is approximately in sync with
356 geophysical time (e.g., the light phase is set from 7 am to 7 pm). We can assume that animals
357 were sacrificed during "core working hours", i.e. between early morning and late afternoon. This
358 would correspond to an approximate time window from ZT2 to ZT10 (which translates, as an
359 example, to 9 am – 5 pm in the authors' current animal facility at the University of Lausanne). In
360 particular the timepoint for which we predict the strongest IRP activity on its rhythmic targets
361 (ZT12; see Fig. 4A) is unlikely to have been included in previously published work, given that it
362 lies at the beginning of the dark phase (7 pm in our facility). Despite decades of research on the
363 IRP/IRE system, specific regulatory effects and mechanisms occurring at the onset of, or during
364 the dark phase may thus have gone unnoticed. Dark phase timepoints are, however, particularly
365 relevant when working with nocturnal species, as this is when mice are most active and ingest
366 most of their food. Also in the knockout and control animals used in our experiments, most activity
367 is seen between ZT12-24 as judged by the *in vivo* recordings of locomotor activity (Fig. 3D, F;
368 lower panels). That particular experiment was conducted using skeleton photoperiod illumination
369 (i.e., for most of the "subjective day", the animal was nevertheless in the dark). Due to the strong
370 acute effects of light on mouse behaviour – suppressing activity and inducing sleep (e.g. [51]) –
371 the partitioning between inactive light and active dark phase would be at least as pronounced in
372 an animal facility under LD12:12.
373
374 *IRP loss affects the regulation of 5' and 3' IRE-containing transcripts in a strongly timepoint-*
375 *specific fashion*

376 Next, we assessed across genotypes and timepoints how 5' IRE-containing transcripts (*Ftl1*, *Fth1*,
377 *Alas2*) were affected in their translation efficiencies (Fig. 5A-C) and 3' IRE-containing *Tfrc* in its
378 RNA abundance (Fig. 5D). In the TE analyses, we observed changes that were not only IRP-
379 specific, but also strongly dependent on timepoint. The most striking observation was the
380 timepoint-specificity of translational derepression in *Ireb2*$^{-/-}$ mice (Fig. 5A-C, right panels). Thus,
381 *Ftl1* and *Fth1* (and to a lower extent *Alas2*) showed strongly increased translation efficiencies
382 (i.e., derepression) in the absence of IREB2/IRP2 during the light phase of the day (ZT5), in line
383 with the model that IREB2/IRP2 is the main IRE-regulating IRP in liver [15-17]. By contrast, at the
384 beginning of the dark phase (ZT12), we observed that TEs were low and near-identical between
385 *Ireb2*$^{-/-}$ and *Ireb2*$^{+/+}$ animals (Fig. 5A-C, right panels). These findings indicated that a repressive
386 mechanism distinct from IREB2/IRP2 was acting on the translation of IRE-containing transcripts
387 specifically at ZT12. This mechanism was unable to compensate for IREB2/IRP2 loss at the light
388 phase timepoint.
389 Timepoint-specific effects in *Ireb2*$^{-/-}$ vs. *Ireb2*$^{+/+}$ animals could also be observed for *Tfrc* (Fig. 5D,
390 right panels). On the one hand, the tendency to reduced *Tfrc* levels in *Ireb2*$^{-/-}$ livers (in line with
391 the model that IRP2 protects *Tfrc* mRNA from degradation) was visible at ZT5. However, at ZT12
392 there was no decrease in *Tfrc* mRNA in the absence of IREB2/IRP2 and rather a trend towards
393 increased abundance. Therefore, similarly to the TE repressive effects seen for 5' IREs, also the
394 mRNA stabilising effect for 3' IRE-containing *Tfrc* did not require IRP2 at the dark-phase
395 timepoint.
396 We next analysed the effects associated with the absence of IRP1 (*Aco1*$^{-/-}$ vs. *Aco1*$^{+/+}$ animals).
397 Previous work has demonstrated that FTL1 protein levels are unchanged in livers of IRP1-
398 deficient mice, including under low- and high-iron diets [15]. Indeed, *Ftl1* TE was overall similar
399 between *Aco1*$^{-/-}$ and *Aco1*$^{+/+}$ animals (Fig. 5A, left panel). For *Fth1* and *Alas2,* some translational
400 derepression was visible at ZT5 and, in particular for *Fth1*, also at ZT12 (Fig. 5B, C, left panels;
401 effects not statistically significant). As a result, the differences between TEs at peak (ZT5) and
402 trough (ZT12) were reduced in *Aco1*$^{-/-}$ vs. *Aco1*$^{+/+}$ animals, indicating slightly blunted amplitudes
403 of rhythmic *Fth1* and *Alas2* translation when ACO1/IRP1 was absent. Finally, changes in *Tfrc*
404 mRNA abundance were overall consistent with the effects seen for *Fth1* and *Alas2* TEs. Thus,
405 *Tfrc* mRNA levels were lower in the absence of IRP1 at both timepoints (Fig. 5D, left panels;
406 statistically significant at ZT5 but not at ZT12 due to the spread seen across biological replicates).
407 We thus concluded that despite the generally held model that IRP1 has little effect on IRE
408 regulation in liver, specific differences between knockouts and controls were apparent. However,

409 these did not reach statistical significance due to the relatively low sample size (3 animals per
410 group) and considerable variability across mice.
411 In summary, the above analyses uncovered a complex relationship between timepoint (ZT5,
412 ZT12) and genotype (*Aco1*$^{-/-}$ vs. *Aco1*$^{+/+}$; *Ireb2*$^{-/-}$ vs. *Ireb2*$^{+/+}$) in the regulation of different IRE-
413 containing mRNAs (*Ftl1, Fth1*, *Alas2*, *Tfrc*). Our data indicate that IRP2 is not solely responsible
414 for IRE regulation in liver. Especially at ZT12, IRP2 actually appears to be dispensable for
415 translational repression. They also reveal that absence of IRP1 affects the regulation of IRE-
416 containing mRNAs and, in several cases, the consequences of IRP1-loss appeared pronounced
417 at ZT12. Taken together, it is conceivable that for these rhythmically regulated transcripts, IRP
418 activities are partitioned according to time-of-day, with IRP2 dominating regulation at ZT5 (light
419 phase) and IRP1 able to act at ZT12 (dark phase).
420
421 *Distinct timepoint-dependent regulation and basal repressed states correlate for core iron*
422 *metabolic vs. other 5' IRE-containing transcripts*
423 Beyond the four transcripts analysed in the previous section, several other mRNAs contain
424 validated IREs (e.g. Fig. 1F, H), and many more have been predicted [52]. A recent study has
425 proposed that across different IRE-containing transcripts in rat liver, translational control through
426 IRPs follows a hierarchy based on different iron concentration set-points at which translational
427 repression occurs [53]. Thus, IRE-containing mRNAs encoding core iron storage factors (e.g.
428 Ferritins) are translationally repressed under normal physiological conditions and chow diet (i.e.,
429 "regular" cellular iron levels; our animals were fed normal chow diet throughout), whereas those
430 mRNAs that encode proteins with broader physiological roles are actively translated under these
431 conditions (e.g. *Aco2*, encoding the TCA cycle enzyme, mitochondrial aconitase). Under iron
432 overload, the former transcripts would undergo derepression, yet the latter only experience very
433 little additional stimulation of translation. In iron deficiency, by contrast, *Aco2* is highly responsive
434 and becomes strongly repressed. Interestingly, it was proposed that IRP1 contributes to this
435 setpoint mechanism through the kinetics of IRP1:IRE dissociation [53].
436 Conceivably, similar mechanisms may also underlie the differences that we observe in rhythmic
437 regulation. Indeed, in the control mice, *Ftl1* and *Fth1* (encoding core iron management proteins)
438 were generally more strongly repressed than *Alas2* (encoding a broader function protein involved
439 in heme biosynthesis) – see TE values in the wild-type animals in Fig. 5A-C that were in the range
440 of -4 to -1 for *Ftl1* and *Fth1*, but around -1.5 to -0.5 for *Alas2*. Please note that TE values are
441 derived from RPF/RNA ratios and can therefore be compared between different transcripts.

442 In order to investigate this phenomenon more globally, we set out to analyse the TEs of other
443 IRE-containing mRNAs in our ribosome profiling datasets. First, we explored the group of
444 transcripts with documented 5' IREs that only presented weak, or no, rhythmicity in our original
445 dataset [6] and that are shown in Fig. 1F. Consistent with the validity of the "setpoint model", these
446 transcripts all showed high basal translation efficiencies (-1 to +0.5) and IRP deficiency led, at
447 most, to modest stimulation of translation (Fig. 5E-G). Thus, in *Ireb2*$^{-/-}$ animals,
448 *Slc40a1/Ferroportin*, *Epas2/Hif2a* and *Aco2* were only weakly altered in their TE at either
449 timepoint (Fig. 5E-G, right panels). In *Aco1/Irp1* knockouts, significant derepression was
450 observable at both ZT5 and ZT12 for *Slc40a1/Ferroportin* (encoding a protein in the core iron
451 metabolic machinery that functions as an iron exporter [53]; Fig. 5E, left panel). For *Epas1/Hif2a*
452 a small effect was apparent at ZT12 (Fig. 5F, left panel; statistically not significant; please note
453 that a previous report had suggested specific *Epas1/Hif2a* regulation through IRP1 in liver [17]).
454 The effect size of de-repression for *Aco2* was quantitatively minimal as well (Fig. 5G, left panel).
455 Finally, we also analysed possible gene expression changes for *Slc11a2/Dmt1*, which bears an
456 IRE in its 3' UTR [21]. *Slc11a2* RNA levels changed in a similar fashion to what we had observed
457 for *Tfrc* upon loss of IRP1 or IRP2 (compare Fig. 5H to Fig. 5D).
458 Next, we set out to classify transcripts in a comprehensive fashion, according to how their
459 translation rates were affected across conditions in our ribo-seq datasets. To this end, we used
460 k-means clustering to partition the transcriptome into overall 15 clusters according to the similarity
461 of their z-score-transformed TE profiles (Fig. 5I and Table S1). Validated IRE-containing
462 transcripts and predicted IRE-like mRNAs (list from [52]) were found in several clusters. The two
463 most rhythmically translated IRE-containing mRNAs, *Ftl1* and *Fth1* – but no other (validated or
464 predicted) IRE transcripts – were found together in a common cluster (cluster 8), where they were
465 grouped in immediate neighbourhood (Fig. 5J, K), consistent with their distinct strongly rhythmic
466 regulation. Another cluster – cluster 13 – contained several 5' IRE transcripts (*Aco2, Alas2,*
467 *Slc40a1*, and predicted IRE-like candidates; see Fig. 5I, L), in line with common regulatory
468 mechanisms and possible similar "set-points". Within cluster 13, the close vicinity of *Alas2* and
469 *Slc40a1*, as compared to the more distant *Aco2* (Fig. 5L), recapitulated the differences in
470 magnitude of derepression seen in the individual transcript analyses shown in Fig. 5C, E, G.
471 In summary, the above analyses support the idea that the observability of rhythmicity on IRE-
472 containing transcripts depends on whether in the basal state, these mRNAs are strongly
473 repressed, which allows for a timepoint-dependent derepression as a function of reduced IRP
474 activity.
475

476 *Feeding-fasting cycles constitute the physiological basis of IRP/IRE rhythmicity*

477 Finally, we wished to understand whether rhythmic IRP/IRE regulation was a *bona fide* circadian
478 clock-driven phenomenon that depended on functional clocks locally in hepatocytes and/or
479 systemically in the whole organism, or if other rhythmicity cues were involved. Briefly, it is well
480 established that various direct and indirect mechanisms, alone or in combination, are involved in
481 driving gene expression oscillations in liver (reviewed in [54]). A considerable proportion of
482 rhythmic mRNA expression is thus driven transcriptionally and directly through the cellular core
483 clock. The transcription of these clock-controlled genes (CCGs) is dependent on the transcription
484 factors that also generate the oscillations within the timekeeping mechanism. However, numerous
485 cases of hepatic gene expression oscillations still persist in the absence of local liver clocks, as
486 they are driven by systemic cues. The underlying mechanisms include, for example, circadian
487 oscillations in body temperature that are generated by the master clock in the SCN and lead to
488 changes in the activity of the transcription factor *Hsf1*, which in turn drives transcriptional
489 oscillations without the obligatory involvement of local hepatocyte clocks [55-57]. Moreover,
490 feeding/fasting cycles – that are a consequence of behavioural rhythmicity and hence an output
491 from the master clock in the SCN – are a particularly important timing cue for liver and other
492 metabolically active peripheral organs. Rhythmic feeding is a well-established *Zeitgeber* for the
493 entrainment of hepatic clocks and, in addition, feeding-dependent signals also regulate gene
494 expression directly, without the need of local hepatocyte clocks. For example, the nutrient-
495 responsive mTOR pathway undergoes daily activation cycles in response to feeding, which
496 regulates the translation of ribosomal protein mRNAs containing regulatory 5' TOP motifs [6, 58,
497 59].

498 In order to explore at which level in the organism a circadian clock was required for IRP/IRE
499 rhythms, we used the oscillations of *Tfrc* mRNA as a proxy for rhythmic IRP/IRE regulation. This
500 allowed us to take advantage of the numerous published around-the-clock RNA-seq datasets
501 from wild-type and clock-deficient mice under a variety of feeding regimes. First, we analysed the
502 RNA-seq data from a recent study [60] that used three different genetic animal models: wild-type,
503 *Bmal1* knockout (i.e., behaviourally arrhythmic with no functional clocks in the entire body) and
504 liver-specific *Bmal1* re-expression (i.e. behaviourally arrhythmic, with functional clock only in
505 hepatocytes), either fed *ad libitum* or night-restricted. Night-restricted feeding exacerbated *Tfrc*
506 rhythmicity in wild-type mice (Fig. 6A, upper). In *Bmal1* KO mice, *Tfrc* was arrhythmic under *ad*
507 *libitum* feeding, yet rhythmicity was re-installed under night-feeding (Fig. 6A, middle) and in *Bmal1*
508 re-expression mice, *Tfrc* regained rhythmicity under night-feeding (Fig. 6A, lower). This data was
509 fully compatible with a model according to which local clocks (liver) or a circadian master clock

510 (SCN) were *per se* not essential for *Tfrc* rhythmicity, as long as feeding-fasting cycles persisted.
511 We confirmed this conclusion in two other datasets. Atger et al. [7] collected livers from night-fed
512 full-body *Bmal1* KO vs. wild-type mice and applied an RNA-seq methodology to quantify both
513 mRNA and pre-mRNA levels. In this experiment, *Tfrc* mRNA rhythms are indistinguishable
514 between the circadian clock-deficient *Bmal1* KO and the control animals under imposed night-
515 feeding (Fig. 6B, upper panel), and pre-mRNA (transcription) is identical and arrhythmic in both
516 genotypes (Fig. 6B, lower panel). We concluded that rhythmic feeding was sufficient to induce
517 post-transcriptionally generated *Tfrc* mRNA oscillations in the absence of an endogenous
518 circadian system. Next, we used the study by Greenwell et al. [61] to investigate the
519 complementary scenario, i.e. how *Tfrc* rhythmicity in liver fares in the presence of a wild-type
520 circadian system, but in the absence of feeding/fasting cycles (Fig. 6C). The analysis of four
521 different feeding regimens from night-restricted (100% food intake during the dark phase) to *ad*
522 *libitum* (~76% during dark), "damped"/almost entirely arrhythmic feeding (~56% during dark) and
523 arrhythmic feeding (~51% of food intake during dark vs. ~49% during light phase), revealed a
524 gradual disappearance of *Tfrc* rhythmicity that scaled with the loss of feeding/fasting cycles (Fig.
525 6C). Finally, we analysed data comprised in the study by Manella et al. [62] in which wild-type
526 mice were subjected to *ad libitum* or to day-restricted feeding under conditions that had little
527 influence on the phase of the liver circadian clock, which revealed that the peak in *Tfrc* mRNA
528 accumulation was inverted and followed feeding rhythms rather than the light-dark cycle (Fig. 6D).
529 From the above analyses that probe the relative importance of the circadian system vs.
530 feeding/fasting cycles for the rhythmic accumulation of *Tfrc*, we can conclude that it is via the
531 latter mechanism – feeding – that *Tfrc* mRNA oscillations are engendered. By extension, we
532 propose that feeding-related timing cues constitute a physiological basis for rhythmicity of the
533 IRP/IRE system in liver tissue.
534

535 **Discussion**

536 Several decades of research have led to a remarkable level of understanding of the IRP/IRE
537 system, which has become a paradigm, and literally a "textbook example" [63], of post-
538 transcriptional gene regulatory control, and which has caught particular attention certainly also
539 due to its relevance for human diseases such as iron storage disorders [44]. Surprisingly, the
540 regulatory feature that we have explored in detail in the current study – differences that are
541 associated with the time-of-day – has nevertheless gone largely unnoticed so far with the
542 exception of a recent preprint that touches on this topic as well [30]. One of our key findings is
543 that high-amplitude rhythmic regulation in the liver is restricted precisely to the subset of

544 transcripts that are archetypes of IRE regulation, namely the Ferritins (*Fth1, Fth2*), *Alas2* and *Tfrc*,
545 which were also historically the first to be discovered [8-10, 20]. Over the years, IREs in many
546 other transcripts have been reported, validated, or predicted – yet for none of them have we
547 observed comparably high peak-to-trough amplitudes across the various datasets that we have
548 analysed. In line with the "set-point model" that has recently been put forward to explain how IRP
549 activity thresholds lead to a hierarchy of translational repression across 5' IRE-containing
550 transcripts [53], the most rhythmically regulated mRNAs are also the most sensitive to repression
551 and generally exhibit lower translation rates (Fig. 5A-C) compared with the non- (or less-)
552 rhythmically regulated transcripts, which are overall more highly translated (Fig. 5E-G). Therefore,
553 we deem it likely that the appearance of rhythmicity for some but not for other IRE-containing
554 transcripts is not necessarily the reflection of principally different molecular mechanism of
555 regulation across these mRNAs, but rather of whether the transcript/IRE-specific thresholds
556 match the physiological dynamic range of regulatory cues that modulate the IRPs. This model
557 would also explain why rhythmic regulation for the same mRNAs is less prominent in the kidney;
558 conceivably, the dynamic range of the cues could simply be different in this organ.
559 An open question that we have not addressed in the framework of this study and that will require
560 future investigations, concerns the identity of the cue that is responsible for imparting rhythmicity.
561 Certainly, a prime candidate would be iron itself, more particularly iron in the so-called "labile iron
562 pool" or LIP, which consists of redox-active iron ions that are weakly liganded and therefore
563 engage in regulatory and metabolic processes [64]. Quantifying the relevant iron pool in tissues
564 is technically not a facile enterprise, given the large amounts of iron that is stored in ferritin or
565 otherwise bound in various Fe-S cluster- or cytochrome-containing proteins, plus the large
566 quantities of iron in the mitochondria and lysosomes. Moreover, in tissue analyses from liver, even
567 minute iron contaminations that can be released from lysed red blood cells (hemoglobin), would
568 likely by far exceed possible rhythmic differences in the relevant intracellular iron pool, making *in*
569 *vivo* measurements a particularly daunting task. Finally, there is ample evidence that additional
570 cues act to regulate IRPs as well, in particular oxygen, reactive oxygen species as well as nitric
571 oxide [42, 65-67]. Interestingly, daily rhythms in tissue $O_2$ [68] and $H_2O_2$ [69] levels have been
572 described. It will thus be important, yet not trivial, to disentangle to what extent these various cues
573 are relevant for rhythmic regulation of IRE-containing transcripts.
574 Another important aspect of our study is that it allows us to refine our understanding of the role of
575 IRP2 in hepatic IRE regulation. While there is indeed a large body of literature supporting the idea
576 that IRP2 is the principle actor in the regulation of Ferritin protein and *Tfrc* mRNA accumulation
577 in liver (e.g. [15-17]), we deem it likely that the vast majority of former studies analysed tissues

578 collected during the light phase of the day. Our examination of time-resolved ribo-seq data indeed
579 confirms that at the light phase timepoint ZT5, knockouts of IRP2 (but not of IRP1) present strong
580 translational depression of Ferritin mRNAs. However, at the dark phase timepoint, ZT12, low
581 translation efficiency is fully maintained even in the absence of IRP2 (Fig. 5A-B), indicating that a
582 different repressor is capable of acting on these IREs at this time-of-day. An obvious candidate is
583 IRP1, whose knockout indeed showed a tendency to derepression at ZT12, at least for *Fth1* (Fig.
584 5B). Since the double deficiency for both IRPs is not viable – even as a conditional, liver-specific
585 knockout [70] – we cannot test the hypothesis that at ZT12, it is the combined activity of IRP1 and
586 IRP2 that acts in repression. Still, based on our data we would propose a model according to
587 which IRP1 is inactive at ZT5, and thus all repression occurs through IRP2 for the light phase
588 timepoint, yet IRP1 and IRP2 are redundantly active at ZT12. In terms of possible molecular
589 mechanisms that could engender higher IRP1 activity at this time point, lower iron levels or
590 changes in one of the other relevant cues could play a role. For example, it is interesting to note
591 that liver $H_2O_2$ levels (a reflection of overall mitochondrial activity) are highest precisely at the
592 light-dark transition [69]. One may thus hypothesize that high $H_2O_2$ could engender the oxidation
593 and destabilisation of IRP1's Fe-S cluster, leading to apo-IRP1 that is capable of binding to IREs.
594 Experimental evidence will be needed to validate such speculations.
595 By leveraging publicly available datasets and using *Tfrc* oscillations as a readout for diurnal
596 IRP/IRE regulation, we also uncovered that rhythmic control does not require a local circadian
597 clock in hepatocytes, nor a central pacemaker in the SCN, as long as rhythmic feeding is
598 maintained (Fig. 6). In animals with a fully intact circadian system, night-restricted feeding readily
599 exacerbated the peak-to-trough amplitude of *Tfrc* abundance oscillations, and it led to some
600 phase delay as compared to *ad libitum* feeding. These observations are in line with the idea of
601 limited direct influence and interference from the circadian clock onto the observed rhythm. The
602 fact that daytime-fed mice have inverted hepatic *Tfrc* rhythms further underscores the dominant
603 role of feeding (Fig. 6D). In this aspect, IRP/IRE rhythmicity distinguishes itself from the rhythmic
604 mechanism acting on ribosomal protein (RP) mRNAs whose translational upregulation occurs
605 also around the light-dark transition in mice fed *ad libitum* or at night [6, 7, 58]. However, in day-
606 fed animals, the rhythm in newly synthesised RPs does not invert but becomes flat [59]. The RP
607 mRNAs contain 5' TOP motifs that are regulated via the mTOR pathway, which shows multiple
608 interactions with clock regulation [71]. A plausible model has emerged according to which the
609 translational upregulation of RP mRNAs by feeding is gated in a circadian fashion, i.e. the feeding
610 signal can exert its stimulatory effect only at a specific time of day. No such circadian gating
611 appears to be in place for the IRP/IRE system, as judged by *Tfrc* mRNA profiles.

612 Conceptually, it is interesting to note that our findings reinforce the idea that rhythmic gene
613 expression is governed by at least two distinct mechanisms. On the one hand, these are truly
614 circadian clock-driven oscillations that are engendered at the transcriptional level and can thus
615 be considered "hard-wired" within the DNA sequence. On the other hand, most post-
616 transcriptional/translational oscillations reported so far appear to reflect the activity of other, acute
617 cues and signals – in particular from feeding. Indeed, translation can be considered an ideal step
618 where such information can be integrated to directly modulate protein output in a rapid and
619 efficient manner. The reactivity of the IRP/IRE system to rhythmic feeding would be a further
620 example for this mechanism.
621

## 622 Materials and methods

### 623 Animals

624 All animal experiments were performed according to the cantonal guidelines of the Canton of
625 Vaud, Switzerland, license VD3402. Healthy adult male mice of age 12-24 weeks were used. All
626 mouse lines were maintained on a C57BL/6J background. The knockout mice for IRP1 (allele
627 *Aco1*$^{tm1.1Mwh}$) and IRP2 (allele *Ireb2*$^{tm1.2Mwh}$) have been described in [72]. Strains kindly provided
628 by Matthias W. Hentze, EMBL Heidelberg.
629

### 630 Protein extraction and Western Blots

631 Total liver protein lysates (*Aco1* and *Ireb2* strains) were prepared as follows: Livers were
632 homogenized in 3 volumes (w/v) of RIPA buffer (150 mM NaCl, 50 mM Tris pH 8.0, 1% NP40,
633 0.5% Na-deoxycholate, 0.1% SDS and Roche complete protease inhibitors) using a Teflon
634 homogenizer, incubated for 30 min on ice and centrifuged for 10 min at 16000 x g and 4°C.
635 Supernatants were stored at -80°C. Protein concentrations were quantified using a BCA protein
636 assay kit (Pierce). For the around-the-clock wild-type and *Smg6* mutant livers, total lysates from
637 our previous study were used that had been prepared by the NUN (NaCl, Urea, Nonidet P-40)
638 procedure, see [29].
639 Immunoblotting to PVDF membrane was carried out using iBlot 2 dry blotting system (Invitrogen).
640 For the blots in Fig 4G and J, bi-directional diffusion transfer that results in two mirror image
641 membranes per gel was carried out (protocol Ulrich Laemmli, personal communication). Briefly,
642 PVDF membranes were placed on both sides of the gel and further sandwiched by 2 pre-wet
643 Whatman filter papers and fibre pads. The stack was placed inside a transfer stack holder and
644 submerged in a tank filled with transfer buffer (Tris-HCl 10 mM pH7.5, EDTA 2 mM, NaCl 50 mM
645 and DTT 0.1 mM) and tightly sealed. The container was then placed in an incubator at 50°C for

646 overnight diffusion transfer. Following transfer, membranes were blocked and incubated with
647 primary and secondary antibodies in 5% milk/TBS-T. For IRP1 and IRP2 Western blots, undiluted
648 crude hybridoma supernatants were used in primary antibody incubation. The dilutions for the
649 remaining antibodies are as follows: anti-Transferrin Receptor (ThermoFisher 13-6800, 1:1000),
650 anti-FBXL5 (ThermoFisher PA5-113529, 1:1000), anti-VINCULIN (Abcam 129002, 1:10000), rat
651 monoclonal anti-ACO1 and anti-IREB2 (undiluted hybridoma supernatant from own preparation);
652 secondary antibodies: anti-rabbit HRP or anti-mouse HRP (Promega, 1:10000).
653
654 **RNA extraction and library preparation**
655 *Library preparation from footprints and total RNA*. The libraries for ribosome profiling were
656 generated as [6] with few modifications. Briefly, frozen liver tissues from individual mice were
657 homogenized with 5-6 strokes using a Teflon homogenizer in 3 volumes of polysome buffer (150
658 mM NaCl, 20 mM Tris-HCl pH7.4, 5 mM $MgCl_2$, 5 mM DTT, complete EDTA-free protease
659 inhibitors (Roche) and 40 U/ml RNasin plus (Promega)) supplemented with 1% Triton X-100 and
660 0.5% Na deoxycholate. Liver lysates were incubated on ice for 10 min and cleared by
661 centrifugation at 10000 g, 4°C for 10 min. Supernatants were flash-frozen and stored in liquid
662 nitrogen. For each sample, 15 $OD_{260}$ of liver lysate was digested with RNase I (Ambion) for 45
663 min at RT under gentle agitation. Digested samples were passed through pre-washed (4x with
664 700 µl polysome buffer for 1 min at 450 x g) Sephacryl S-400 HR spin columns (GE healthcare,
665 currently Cytiva), and centrifuged for 2 min at 450 x g at 4°C. The resulting flow-through was
666 mixed with Qiazol and ribosome-protected fragments (RPFs) were purified using miRNeasy RNA
667 extraction kit (Qiagen) according to the manufacturer's instructions. Total RNA was extracted from
668 undigested liver lysates using Qiazol and miRNeasy kit in parallel to generate total RNA libraries.
669 1 µg of RPF and total RNA samples were depleted of ribosomal RNA using RiboCop rRNA
670 depletion kit V1.3 (Lexogen), followed by purification with RNA Clean & Concentrator-5 (Zymo
671 research). All the subsequent steps were performed according to Illumina's TruSeq Ribo-Profile
672 protocol with minor modifications as described in [73]. Size-selection of fragments at different
673 steps was as follows: ribosome-protected fragments (RPFs) were size-separated on 15% urea-
674 polyacrylamide gels and excised at a size range of 24-36 nt (monosome footprint). The cDNA
675 fragments generated from RPFs and total RNA were separated on 10% urea-polyacrylamide gels
676 and excised at a size range of 70-80 nt and 70-100 nt, respectively. The PCR-amplified libraries
677 were size-selected on 8% native polyacrylamide gels. Monosome libraries were at ~150 bp and
678 total RNA libraries were at ~150 to 170 nt. All libraries were sequenced on Illumina HiSeq 2500.
679

680 *Ribosome profiling data analysis.* Sequencing reads were mapped following overall the
681 strategy described in [6]. Adapter sequences were removed from the sequenced reads using
682 cutadapt (v3.5) with the following options: --match-read-wildcards --overlap 8 --discard-untrimmed
683 --minimum-length 30 and reads were quality filtered using fastx_toolkit (-Q33 -q 30 -p 90).
684 Trimmed read sequences were filtered by their size using an in-house Python script with following
685 inclusive ranges: [26,35] for footprints, [21,60] for total RNA. Reads were then mapped to rRNA
686 and tRNA databases to remove contaminants using bowtie2 (-p 2 -L 15 -k 20 --no-unal -q). Only
687 reads that did not map to the above databases were mapped to mouse genome v38.100 using
688 STAR (version 2.70f). Read counts of total RNA and RPF were normalized with upper quantile
689 method of R package edgeR v3.4.2 [74]. Translational efficiencies (TE) were calculated on
690 normalised reads as the ratio of RPF / mRNA for each gene per sample. TEs were $log_2$-
691 transformed and plotted for comparing means of replicates per time point for each genotype. K-
692 Means cluster analysis was performed on the different conditions (averaged by replicates). Based
693 on the Within-Cluster-Sum of Squared Errors, the number of clusters was fixed to 15 sets.
694 Hierarchical clustering was then performed within individual clusters to assess proximity between
695 genes of a given cluster.
696
697 **Liver explant preparation and bioluminescence recording**
698 For explant preparation, male IRP1 or IRP2 KO and matched control animals from the same
699 breedings (i.e., same genetic background) were euthanized following deep anaesthesia by
700 isoflurane inhalation. Liver tissue was excised and placed immediately in ice-cold Hank's buffer
701 (Thermo Fisher Scientific). The outermost edges of the tissue were carefully excised in a sterile
702 cabinet, and immediately placed on a 0.4 micron Millicell cell culture inserts (PICMORG50) in a
703 35 mm dish with phenol-free DMEM (Thermo Fisher Scientific, 11880028) containing 5% FBS, 2
704 mM glutamine, 100 U/ml penicillin, 100 µg/ml streptomycin and 0.1 mM luciferin. The parafilm-
705 sealed plates were placed for recording in the LumiCycler (Actimetrics) at 37°C and 5% CO2.
706
707 ***In vivo* recording in the RT-Biolumicorder**
708 Adult male mice, 12-20 weeks of age, carrying the genetically encoded circadian reporter allele
709 *mPer2::Luc* [50] and deficient for *Aco1* or *Ireb2* were used for the RT-Biolumicorder experiments,
710 along with controls, i.e. wild-type male mice from the same breedings/with the same genetic
711 background and of the same age. The experimental procedure followed our previously published
712 protocols [49]. Briefly, ALZET mini-osmotic pumps were filled with D-luciferin sodium salt and
713 closed with blue-coloured flow moderators (ALZET) under sterile conditions. The pumps were

activated at 37°C according to the manufacturer's instructions, followed by subcutaneous, dorsal implantation. Before implantation, the dorsal area of the mouse at the site where the liver is positioned was shaved using an electric razor. The RT-Biolumicorder (Lesa-Technology) consists of a cylindrical cage equipped with a photomultiplier tube (PMT) allowing for recording of real-time longitudinal bioluminescence from single-housed mice. The data, which also contain locomotor activity traces, light and food access information, were saved as text files and analysed using the MATLAB-based "Osiris" software according to [49].

**Acknowledgements**

We thank Matthias W. Hentze for knockout mouse strains; the Lausanne Genomic Technologies Facility for library preparation and sequencing; and Paul Franken and members of the Gatfield lab for comments on the manuscript.

**Funding**

Swiss National Science Foundation (SNSF), NCCR RNA & Disease grant 141735 (DG)
Swiss National Science Foundation (SNSF) individual grant 179190 (DG)

**Competing interests:** Authors declare that they have no competing interests.

**Data and Materials Availability:** All data needed to evaluate the conclusions in the paper are present in the paper and/or the Supplementary Materials. Sequencing data have been deposited at GEO (GSE243134) with reviewer token (suppressed).

## References

1. Cox, K.H. and J.S. Takahashi, *Circadian clock genes and the transcriptional architecture of the clock mechanism.* J Mol Endocrinol, 2019. **63**(4): p. R93-R102.
2. Partch, C.L., C.B. Green, and J.S. Takahashi, *Molecular architecture of the mammalian circadian clock.* Trends Cell Biol, 2014. **24**(2): p. 90-9.
3. Bolshette, N., et al., *Circadian regulation of liver function: from molecular mechanisms to disease pathophysiology.* Nat Rev Gastroenterol Hepatol, 2023.
4. Crosby, P. and C.L. Partch, *New insights into non-transcriptional regulation of mammalian core clock proteins.* J Cell Sci, 2020. **133**(18).
5. Castelo-Szekely, V. and D. Gatfield, *Emerging Roles of Translational Control in Circadian Timekeeping.* J Mol Biol, 2020. **432**(12): p. 3483-3497.

748 6. Janich, P., et al., *Ribosome profiling reveals the rhythmic liver translatome and circadian*
749 *clock regulation by upstream open reading frames.* Genome Res, 2015. **25**(12): p. 1848-
750 59.
751 7. Atger, F., et al., *Circadian and feeding rhythms differentially affect rhythmic mRNA*
752 *transcription and translation in mouse liver.* Proc Natl Acad Sci U S A, 2015. **112**(47): p.
753 E6579-88.
754 8. Hentze, M.W., et al., *Identification of the iron-responsive element for the translational*
755 *regulation of human ferritin mRNA.* Science, 1987. **238**(4833): p. 1570-3.
756 9. Aziz, N. and H.N. Munro, *Both subunits of rat liver ferritin are regulated at a translational*
757 *level by iron induction.* Nucleic Acids Res, 1986. **14**(2): p. 915-27.
758 10. Dandekar, T., et al., *Identification of a novel iron-responsive element in murine and human*
759 *erythroid delta-aminolevulinic acid synthase mRNA.* EMBO J, 1991. **10**(7): p. 1903-9.
760 11. Kaasik, K. and C.C. Lee, *Reciprocal regulation of haem biosynthesis and the circadian*
761 *clock in mammals.* Nature, 2004. **430**(6998): p. 467-71.
762 12. Anderson, C.P., et al., *Mammalian iron metabolism and its control by iron regulatory*
763 *proteins.* Biochim Biophys Acta, 2012. **1823**(9): p. 1468-83.
764 13. Muckenthaler, M.U., et al., *A Red Carpet for Iron Metabolism.* Cell, 2017. **168**(3): p. 344-
765 361.
766 14. Galy, B., M. Conrad, and M. Muckenthaler, *Mechanisms controlling cellular and systemic*
767 *iron homeostasis.* Nat Rev Mol Cell Biol, 2023.
768 15. Meyron-Holtz, E.G., et al., *Genetic ablations of iron regulatory proteins 1 and 2 reveal why*
769 *iron regulatory protein 2 dominates iron homeostasis.* EMBO J, 2004. **23**(2): p. 386-95.
770 16. Cooperman, S.S., et al., *Microcytic anemia, erythropoietic protoporphyria, and*
771 *neurodegeneration in mice with targeted deletion of iron-regulatory protein 2.* Blood, 2005.
772 **106**(3): p. 1084-91.
773 17. Anderson, S.A., et al., *The IRP1-HIF-2alpha axis coordinates iron and oxygen sensing*
774 *with erythropoiesis and iron absorption.* Cell Metab, 2013. **17**(2): p. 282-90.
775 18. Campillos, M., et al., *SIREs: searching for iron-responsive elements.* Nucleic Acids Res,
776 2010. **38**(Web Server issue): p. W360-7.
777 19. Sanchez, M., et al., *Iron regulatory protein-1 and -2: transcriptome-wide definition of*
778 *binding mRNAs and shaping of the cellular proteome by iron regulatory proteins.* Blood,
779 2011. **118**(22): p. e168-79.

780 20. Casey, J.L., et al., *Iron regulation of transferrin receptor mRNA levels requires iron-*
781 *responsive elements and a rapid turnover determinant in the 3' untranslated region of the*
782 *mRNA.* EMBO J, 1989. **8**(12): p. 3693-9.
783 21. Gunshin, H., et al., *Iron-dependent regulation of the divalent metal ion transporter.* FEBS
784 Lett, 2001. **509**(2): p. 309-16.
785 22. Luscieti, S., et al., *The actin-binding protein profilin 2 is a novel regulator of iron*
786 *homeostasis.* Blood, 2017. **130**(17): p. 1934-1945.
787 23. Castelo-Szekely, V., et al., *Translational contributions to tissue specificity in rhythmic and*
788 *constitutive gene expression.* Genome Biol, 2017. **18**(1): p. 116.
789 24. Lymboussaki, A., et al., *The role of the iron responsive element in the control of*
790 *ferroportin1/IREG1/MTP1 gene expression.* J Hepatol, 2003. **39**(5): p. 710-5.
791 25. Gray, N.K., et al., *Translational regulation of mammalian and Drosophila citric acid cycle*
792 *enzymes via iron-responsive elements.* Proc Natl Acad Sci U S A, 1996. **93**(10): p. 4925-
793 30.
794 26. Sanchez, M., et al., *Iron-regulatory proteins limit hypoxia-inducible factor-2alpha*
795 *expression in iron deficiency.* Nat Struct Mol Biol, 2007. **14**(5): p. 420-6.
796 27. Le Martelot, G., et al., *Genome-wide RNA polymerase II profiles and RNA accumulation*
797 *reveal kinetics of transcription and associated epigenetic changes during diurnal cycles.*
798 PLoS biology, 2012. **10**(11): p. e1001442.
799 28. Du, N.H., et al., *MicroRNAs shape circadian hepatic gene expression on a transcriptome-*
800 *wide scale.* Elife, 2014. **3**: p. e02510.
801 29. Katsioudi, G., et al., *A conditional Smg6 mutant mouse model reveals circadian clock*
802 *regulation through the nonsense-mediated mRNA decay pathway.* Sci Adv, 2023. **9**(2): p.
803 eade2828.
804 30. Bennett, C., et al., *Serum iron and hepatic transferrin receptor expression are circadian-*
805 *regulated.* bioRxiv, 2023: p. 2023.05.07.539729.
806 31. Miyazawa, M., et al., *Regulation of transferrin receptor-1 mRNA by the interplay between*
807 *IRE-binding proteins and miR-7/miR-141 in the 3'-IRE stem-loops.* RNA, 2018. **24**(4): p.
808 468-479.
809 32. Corral, V.M., et al., *Roquin is a major mediator of iron-regulated changes to transferrin*
810 *receptor-1 mRNA stability.* iScience, 2021. **24**(4): p. 102360.
811 33. Yoshinaga, M., et al., *Regnase-1 Maintains Iron Homeostasis via the Degradation of*
812 *Transferrin Receptor 1 and Prolyl-Hydroxylase-Domain-Containing Protein 3 mRNAs.* Cell
813 Rep, 2017. **19**(8): p. 1614-1630.

814 34. Mino, T., et al., *Translation-dependent unwinding of stem-loops by UPF1 licenses*
815 *Regnase-1 to degrade inflammatory mRNAs.* Nucleic Acids Res, 2019. **47**(16): p. 8838-
816 8859.
817 35. Zhu, X., H. Zhang, and J.T. Mendell, *Ribosome Recycling by ABCE1 Links Lysosomal*
818 *Function and Iron Homeostasis to 3' UTR-Directed Regulation and Nonsense-Mediated*
819 *Decay.* Cell Rep, 2020. **32**(2): p. 107895.
820 36. Fader, K.A., et al., *Corrigendum to "Convergence of hepcidin deficiency, systemic iron*
821 *overloading, heme accumulation, and REV-ERBalpha/beta activation in aryl hydrocarbon*
822 *receptor-elicited hepatotoxicity" [Toxicol. Appl. Pharmacol. 321 (2017) 1-17].* Toxicol Appl
823 Pharmacol, 2018. **344**: p. 74.
824 37. Okazaki, F., et al., *Circadian Clock in a Mouse Colon Tumor Regulates Intracellular Iron*
825 *Levels to Promote Tumor Progression.* J Biol Chem, 2016. **291**(13): p. 7017-28.
826 38. Ripperger, J.A. and U. Schibler, *Rhythmic CLOCK-BMAL1 binding to multiple E-box motifs*
827 *drives circadian Dbp transcription and chromatin transitions.* Nat Genet, 2006. **38**(3): p.
828 369-74.
829 39. Vashisht, A.A., et al., *Control of iron homeostasis by an iron-regulated ubiquitin ligase.*
830 Science, 2009. **326**(5953): p. 718-21.
831 40. Salahudeen, A.A., et al., *An E3 ligase possessing an iron-responsive hemerythrin domain*
832 *is a regulator of iron homeostasis.* Science, 2009. **326**(5953): p. 722-6.
833 41. Terzi, E.M., et al., *Iron-sulfur cluster deficiency can be sensed by IRP2 and regulates iron*
834 *homeostasis and sensitivity to ferroptosis independent of IRP1 and FBXL5.* Sci Adv, 2021.
835 **7**(22).
836 42. Meyron-Holtz, E.G., M.C. Ghosh, and T.A. Rouault, *Mammalian tissue oxygen levels*
837 *modulate iron-regulatory protein activities in vivo.* Science, 2004. **306**(5704): p. 2087-90.
838 43. Galy, B., D. Ferring, and M.W. Hentze, *Generation of conditional alleles of the murine Iron*
839 *Regulatory Protein (IRP)-1 and -2 genes.* Genesis, 2005. **43**(4): p. 181-8.
840 44. Wilkinson, N. and K. Pantopoulos, *The IRP/IRE system in vivo: insights from mouse*
841 *models.* Front Pharmacol, 2014. **5**: p. 176.
842 45. Yin, L., et al., *Rev-erbalpha, a heme sensor that coordinates metabolic and circadian*
843 *pathways.* Science, 2007. **318**(5857): p. 1786-9.
844 46. Andreini, C., et al., *The human iron-proteome.* Metallomics, 2018. **10**(9): p. 1223-1231.
845 47. Liu, J., et al., *Iron accumulation with age alters metabolic pattern and circadian clock gene*
846 *expression through the reduction of AMP-modulated histone methylation.* J Biol Chem,
847 2022. **298**(6): p. 101968.

848 48. Saini, C., et al., *Real-time recording of circadian liver gene expression in freely moving*
849 *mice reveals the phase-setting behavior of hepatocyte clocks.* Genes Dev, 2013. **27**(13):
850 p. 1526-36.
851 49. Katsioudi, G., et al., *Recording of Diurnal Gene Expression in Peripheral Organs of Mice*
852 *Using the RT-Biolumicorder.* Methods Mol Biol, 2022. **2482**: p. 217-242.
853 50. Yoo, S.H., et al., *PERIOD2::LUCIFERASE real-time reporting of circadian dynamics*
854 *reveals persistent circadian oscillations in mouse peripheral tissues.* Proc Natl Acad Sci
855 U S A, 2004. **101**(15): p. 5339-46.
856 51. Tsai, J.W., et al., *Melanopsin as a sleep modulator: circadian gating of the direct effects*
857 *of light on sleep and altered sleep homeostasis in Opn4(-/-) mice.* PLoS Biol, 2009. **7**(6):
858 p. e1000125.
859 52. Volz, K., *Conservation in the Iron Responsive Element Family.* Genes (Basel), 2021.
860 **12**(9).
861 53. Garza, K.R., et al., *Differential translational control of 5' IRE-containing mRNA in response*
862 *to dietary iron deficiency and acute iron overload.* Metallomics, 2020. **12**(12): p. 2186-
863 2198.
864 54. Dibner, C., U. Schibler, and U. Albrecht, *The mammalian circadian timing system:*
865 *organization and coordination of central and peripheral clocks.* Annu Rev Physiol, 2010.
866 **72**: p. 517-49.
867 55. Reinke, H., et al., *Differential display of DNA-binding proteins reveals heat-shock factor 1*
868 *as a circadian transcription factor.* Genes Dev, 2008. **22**(3): p. 331-45.
869 56. Buhr, E.D., S.H. Yoo, and J.S. Takahashi, *Temperature as a universal resetting cue for*
870 *mammalian circadian oscillators.* Science, 2010. **330**(6002): p. 379-85.
871 57. Saini, C., et al., *Simulated body temperature rhythms reveal the phase-shifting behavior*
872 *and plasticity of mammalian circadian oscillators.* Genes Dev, 2012. **26**(6): p. 567-80.
873 58. Jouffe, C., et al., *The circadian clock coordinates ribosome biogenesis.* PLoS Biol, 2013.
874 **11**(1): p. e1001455.
875 59. Sinturel, F., et al., *Diurnal Oscillations in Liver Mass and Cell Size Accompany Ribosome*
876 *Assembly Cycles.* Cell, 2017. **169**(4): p. 651-663 e14.
877 60. Greco, C.M., et al., *Integration of feeding behavior by the liver circadian clock reveals*
878 *network dependency of metabolic rhythms.* Sci Adv, 2021. **7**(39): p. eabi7828.
879 61. Greenwell, B.J., et al., *Rhythmic Food Intake Drives Rhythmic Gene Expression More*
880 *Potently than the Hepatic Circadian Clock in Mice.* Cell Rep, 2019. **27**(3): p. 649-657 e5.

881 62. Manella, G., et al., *The liver-clock coordinates rhythmicity of peripheral tissues in response*
882 *to feeding.* Nat Metab, 2021. **3**(6): p. 829-842.
883 63. Lodish, H.F., *Molecular Cell Biology*. 2000: W.H. Freeman.
884 64. Kakhlon, O. and Z.I. Cabantchik, *The labile iron pool: characterization, measurement, and*
885 *participation in cellular processes(1).* Free Radic Biol Med, 2002. **33**(8): p. 1037-46.
886 65. Weiss, G., et al., *Translational regulation via iron-responsive elements by the nitric*
887 *oxide/NO-synthase pathway.* EMBO J, 1993. **12**(9): p. 3651-7.
888 66. Pantopoulos, K., G. Weiss, and M.W. Hentze, *Nitric oxide and oxidative stress (H2O2)*
889 *control mammalian iron metabolism by different pathways.* Mol Cell Biol, 1996. **16**(7): p.
890 3781-8.
891 67. Pantopoulos, K. and M.W. Hentze, *Rapid responses to oxidative stress mediated by iron*
892 *regulatory protein.* EMBO J, 1995. **14**(12): p. 2917-24.
893 68. Adamovich, Y., et al., *Rhythmic Oxygen Levels Reset Circadian Clocks through*
894 *HIF1alpha.* Cell Metab, 2017. **25**(1): p. 93-101.
895 69. Pei, J.F., et al., *Diurnal oscillations of endogenous H(2)O(2) sustained by p66(Shc)*
896 *regulate circadian clocks.* Nat Cell Biol, 2019. **21**(12): p. 1553-1564.
897 70. Galy, B., et al., *Iron regulatory proteins secure mitochondrial iron sufficiency and function.*
898 Cell metabolism, 2010. **12**(2): p. 194-201.
899 71. Cao, R., *mTOR Signaling, Translational Control, and the Circadian Clock.* Front Genet,
900 2018. **9**: p. 367.
901 72. Galy, B., et al., *Targeted mutagenesis of the murine IRP1 and IRP2 genes reveals context-*
902 *dependent RNA processing differences in vivo.* RNA, 2004. **10**(7): p. 1019-25.
903 73. Arpat, A.B., et al., *Transcriptome-wide sites of collided ribosomes reveal principles of*
904 *translational pausing.* Genome Res, 2020. **30**(7): p. 985-999.
905 74. Robinson, M.D. and A. Oshlack, *A scaling normalization method for differential expression*
906 *analysis of RNA-seq data.* Genome Biol, 2010. **11**(3): p. R25.

907

908

909 ## Figure Legends

910 **Figure 1. Translational rhythmicity is detected on IRE-containing mRNAs in a transcript-**
911 **and tissue-specific fashion.**

912 (**A**) Schematic of the dataset collection carried out for the studies [6, 23] for the liver and kidney
913 gene expression graphs shown in this Figure.

914 (**B**) Schematic model of IRP activity on IREs. Thus, IRP1 can bind to IRE hairpins under conditions
915 of low iron availability. When iron is abundant, it assembles an Fe-S cluster and the protein
916 becomes cytoplasmic Aconitase (Aco1). In this state, it does not bind IREs anymore. For IRP2,
917 there is an iron-dependent degradation pathway that relies on an iron-sensor F-box protein,
918 FBXL5.

919 (**C**) IREs in 5' UTRs and 3' UTRs act by different mechanisms (schematic): When in the 5' UTR,
920 IRP-bound IREs inhibit scanning ribosomes from accessing the initiation codon, thus leading to
921 translational repression. After removal of IRP binding, ribosomes can translate the coding
922 sequence (upper). For 3' UTR IREs, the binding of IRPs inhibits access to endonucleases
923 (depicted as red scissors) that would otherwise initiate transcript degradation. When IRPs
924 dissociate, the mRNA is thus destabilised and becomes less abundant (lower).

925 (**D**) Schematic of the IRE hairpin consensus sequence and structure. IREs are about 35 nt in
926 length Iand are characterized by an apical 6-nt loop motif 5'-CAGWGH-3' (W = A or T and H = A,
927 C or T), and two stem regions (N5 upper stem and variable lower stem) that are separated by a
928 unpaired C bulge. Colour code depicts sequence conservation across IREs from high (blue) to
929 medium (orange) and low (olive).

930 (**E**) RPKM values of CDS-mapping ribosome protected fragment (RPF) data (blue) and RNA-seq
931 data (orange) from the datasets of [6, 23] for the transcripts *Ftl1, Fth1* and *Alas2* around the 24-
932 h daily cycle in liver (upper) and kidney (lower). All three genes show high amplitude translation
933 in liver. Means per timepoint are plotted; "error bars"/vertical lines connect the two biological
934 replicates. Dashed lines represent rhythmic curve fittings to the data, as described in [6].

935 (**F**) As in panel (E), but for the non-/less-rhythmically translated IRE-containing transcripts
936 *Slc40a1/Ferroportin, Aco2, Epas1/Hif2-alpha*.

937 (**G**) Sequence and predicted structure, as well as relative position within 5' UTR, of the IREs of
938 the murine transcripts shown in (E). Colour code as in (D).

939 (**H**) As in (G), but for the transcripts that are shown in panel (F).

940 **Figure 2. Correspondence between *Tfrc* mRNA rhythms and translational oscillations are**
941 **consistent with diurnal IRP activity.**
942 (**A**) Sequence and predicted hairpin structures of the five IREs annotated within the mouse *Tfrc*
943 3' UTR. Nucleotide distances from the TAA stop codon, between individual haipins, and to the
944 annotated transcript end are noted in grey.
945 (**B**) RPKM values of CDS-mapping ribosome protected fragment (RPF) data (blue) and RNA-seq
946 data (orange) from the datasets of [6, 23] for the *Tfrc* transcript around the 24-h daily cycle in liver
947 (upper) and kidney (lower). Means per timepoint are plotted; "error bars"/vertical lines connect the
948 two biological replicates. Dashed lines represent rhythmic curve fittings to the data, as described
949 in [6].
950 (**C**) Expression plots (RPKM) showing around-the-clock data from [28] for *Tfrc* mRNA (exonic
951 reads; upper panel) and pre-mRNA (intronic reads; lower panel) in control (blue) and miRNA-
952 deficient (*Dicer* KO) livers (yellow). Means per timepoint are plotted; "error bars"/vertical lines
953 connect the two biological replicates. The two time series are plotted together in the same graph
954 (vertical lines connect the data points from the two series). Rhythms are seen for mRNA but not
955 for pre-mRNA, indicating that oscillations are post-transcriptionally generated (RNA stability).
956 Dashed lines represent rhythmic curve fittings to the data, as described in [28].
957 (**D**) Expression plots for around-the-clock RNA-seq data from [29] for *Tfrc* showing mRNA (top
958 panel; exonic reads) and pre-mRNA (bottom panel; intronic reads) for *Smg6* mutants (yellow) and
959 controls (blue). RPKM values (reads per kilobase of transcript per million mapped reads) of
960 individual mouse livers are shown as dots with solid lines connecting the means across time
961 points. Dashed lines represent rhythmic curve fittings to the data, as described in [29].
962 (**E**) Western blot analysis of total liver proteins (pool of three mice per sample), for TFRC and
963 VINCULIN (loading control), from control mice (blue; on left side) and *Smg6* mutant mice (yellow;
964 on right side). Same samples as in [29] were used.
965 (**F**) Quantification of Western blot from (E). TFRC itensities were normalised to control band
966 intensities (VINCULIN). The 1.4x upregulation refers to the mean signal in *Smg6* mutants vs.
967 controls.
968 (**G**) Schematic representation of the model that can be deduced from the gene expression data
969 from Fig. 1E (rhythmic translation of *Ftl1, Fth1* and *Alas2*) and Fig. 2B-D (rhythmic mRNA
970 abundance of *Tfrc*). The observed rhythms are thus consistent with IRP activity being minimal
971 and maximal at the light-phase timepoint ZT5 and the light-dark transition timepoint ZT12,
972 respectively.

973 (**H**) As in panel (B), RPKM values of CDS-mapping ribosome protected fragment (RPF) data
974 (blue) and RNA-seq data (orange) from the datasets of [6, 23] for the transcripts *Aco1* (encoding
975 IRP1) and *Ireb2* (encoding IRP2) around the 24-h daily cycle in liver (upper) and kidney (lower).
976 Means per timepoint are plotted; "error bars"/vertical lines connect the two biological replicates.
977 Dashed lines represent rhythmic curve fittings to the data, as described in [6].
978 (**I**) Expression plots (RPKM) showing around-the-clock data from [28] for the indicated transcripts,
979 *Aco1* and *Ireb2,* for mRNA (exonic reads; blue) and pre-mRNA (intronic reads; magenta) in control
980 livers. The data from the miRNA-deficient (*Dicer* KO) livers were ommitted from these analyses.
981 Means per timepoint are plotted; "error bars"/vertical lines connect the two biological replicates.
982 Dashed lines represent rhythmic curve fittings to the data, as described in [28].
983 (**J**) As in (I), but for transcripts *Arntl/Bmal1* and *Dbp.*
984 (**K**) Western blot analysis of total liver proteins as in (E), for ACO1/IRP1 and VINCULIN (loading
985 control).
986 (**L**) Quantification of Western blot from (K). ACO1/IRP1 itensities were normalised to control band
987 intensities (VINCULIN).
988 (**M**) Western blot analysis of total liver proteins from individual animals for IREB2/IRP2; the same
989 extracts that constituted the pools ZT4 and ZT12 (control series) in panel N were used.
990 (**N**) Western blot analysis of total liver proteins as in (E), for IREB2/IRPs and VINCULIN (loading
991 control).
992 (**O**) Quantification of Western blot from (N). IREB2/IRP2 itensities were normalised to control band
993 intensities (VINCULIN).
994 (**P**) Quantification of Western blot from individual livers at ZT4 and ZT12 from (M). IREB2/IRP2
995 itensities were normalised to control band intensities (VINCULIN). Statistical significance
996 evaluated via Student's t-test.
997 (**Q**) Western blot analysis for FBXL5 and VINCULIN (loading control) in total liver proteins from
998 the control series samples from [29]. Left side of blot: around-the-clock, pool of three mice per
999 sample; right side: individiual mice, as in panel (M).
1000 (**R**) Quantification of around-the-clock data from Western blot from (Q). FBXL5 itensities were
1001 normalised to control band intensities (VINCULIN).
1002 (**S**) Quantification of Western blot from individual livers at ZT4 and ZT12 from (Q), right part of
1003 blot. FBXL5 itensities were normalised to control band intensities (VINCULIN). Statistical
1004 significance evaluated via Student's t-test.

1005 **Figure 3. *In vivo* bioluminescence recoding shows that entrained circadian rhythms in liver**
1006 **are unperturbed in mice that are deficient for *Aco1* or *Ireb2*.**
1007 (**A**) Cartoon depicting the *in vivo* recording setup (RT-Biolumicorder) used to measure diurnal
1008 bioluminescence rhythms in freely moving mice. The mouse is implanted with a luciferin-charged
1009 osmotic minipump and dorsally shaved to ensure detectability of photons emitted from the liver.
1010 It is then placed in the arena of the RT-Biolumicorder that records photons via a photomultiplier
1011 tube (PMT), activity via infrared detection, and also offers the possibility to program food
1012 availability and illumination.
1013 (**B**) Schematic representation of the applied recording protocol in the RT-Biolumicorder setup.
1014 Mice expressing the *Per2::Luc* reporter and implanted with the minipump are placed in the RT-
1015 Biolumicorder where they are first subject to LD12:12 schedule and *ad libitum* feeding for 1-2
1016 days, allowing for acclimatisation to the setup. Bioluminescence recording only occurs during the
1017 dark phase. Then, the illumination schedule is changed to skeleton photoperiod (i.e. two 30 min
1018 light pulses applied at times corresponding to the beginning and to the end of the light phase in a
1019 12h-light-12h-dark (LD12:12) cycle). Recording occurs throughout the day with the exception of
1020 the duration of the 30 min light pulses. The skeleton photoperiod is important as it keeps the SCN
1021 clock entrained to a defined 24-hour T-cycle, allowing to specifically query potential changes in
1022 the entrained liver clock,
1023 (**C**) Bioluminescence rhythms and activity traces recorded with the protocol shown in (B) from
1024 mice deficient for *Aco1* (ochre, N=2) and controls (grey, N=2). Mean signal (solid trace) and SEM
1025 (shaded) over the whole course of the experiment are shown.
1026 (**D**) Compiled data of (C), averaging all cycles from day 3. No change in PER2::LUC phase was
1027 detectable between genotypes.
1028 (**E**) Bioluminescence rhythms and activity traces recorded with the protocol shown in (B) from
1029 mice deficient for *Ireb2* (purple, N=4) and controls (grey, N=4). Mean signal (solid trace) and SEM
1030 (shaded) over the whole course of the experiment are shown.
1031 (**F**) Compiled data of (E), averaging all cycles from day 3, For *Ireb2*$^{-/-}$ mice, PER2::LUC peak and
1032 trough phases were slightly delayed as compared to the control mice with the same genetic
1033 background.
1034 (**G**) Schematic of liver explant rhythm measurements from the two genotypes, *Ireb2*$^{-/-}$ and
1035 controls, using male mice from the same breedings. Mice carried the *Per2::Luc* reporter allele.
1036 (**H**) Liver explant bioluminescence recording from *Ireb2*$^{-/-}$ (purple) and control (grey) mice. Free-
1037 running circadian traces show mean signal and SEM for the two genotype over a recording period
1038 of 96 hours. N=10 per genotype.

1039 (**I**) Period length quantification of experiments shown in (H). No significant change in period length
1040 was detectable. *Ireb2* knockout period lengths appeared more variable than controls.

1041 **Figure 4. Time-resolved datasets allow analysis of IRP1 vs. IRP2-dependence of rhythmic**
1042 **regulation.**
1043 (**A**) Schematic representation of the conclusions drawn from the rhythmic analyses of Fig. 1-2
1044 regarding the timing of IRP activity and the selection of timepoints for the ribo-seq experiment.
1045 Thus, high *Ftl1, Fth1* and *Alas2* translation efficiency and low *Tfrc* abundance, conceivably as a
1046 result of mRNA instability, occur in the light phase of the day, allowing us to predict generally low
1047 IRP activity around ZT5. By contrast, low *Ftl1, Fth1* and *Alas2* translation efficiency and the rise
1048 in *Tfrc* abundance at the light-dark transition suggests high IRP activity at ZT12.
1049 (**B**) Schematic of the experiment carried out to assess timepoint- and genotype-specific ribosome
1050 profiling in the two IRP-deficient mouse strains and matched controls. Thus, 3 animals each were
1051 sacrificed at ZT5 and ZT12, for genotypes *Aco1*$^{+/+}$ (dark grey), *Aco1*$^{-/-}$ (ochre), *Ireb2*$^{+/+}$ (light grey),
1052 *Ireb2*$^{-/-}$ (purple). Livers were further processed for ribo-seq and RNA-seq.
1053 (**C**) Quantification of ribosome protected fragments (RPF, top) and RNA abundance (middle) and
1054 relative translation efficiency ($\log_2$ ratio of RPF/RNA) for the *Aco1* transcript in *Aco1* knockout
1055 mice and their matched controls, for the two timepoints ZT5 and ZT12. Read count is normalised
1056 to library depth. Statistical significance evaluated by unpaired t-test and indicated with asterisks
1057 (*** $P < 0.001$, ** $P < 0.01$, * $P < 0.05$).
1058 (**D**) As in (C), for the *Aco1* transcript in *Ireb2* knockout mice and their matched controls.
1059 (**E**) Quantification of ribosome protected fragments (RPF, top) and RNA abundance (middle) and
1060 relative translation efficiency ($\log_2$ ratio of RPF/RNA) for the *Ireb2* transcript in *Aco1* knockout
1061 mice and their matched controls, for the two timepoints ZT5 and ZT12. Read count is normalised
1062 to library depth. Statistical significance evaluated by unpaired t-test and indicated with asterisks
1063 (** $P < 0.001$, ** $P < 0.01$, * $P < 0.05$).
1064 (**F**) As in (E), for the *Ireb2* transcript in *Ireb2* knockout mice and their matched controls.
1065 (**G**) Western blot analysis of total protein extracts from the livers used for the gene expression
1066 profiling in panels (C) and (D), i.e. the *Aco1*$^{-/-}$ and matched *Aco1*$^{+/+}$ mice. VINCULIN was used as
1067 loading control to normalise ACO1/IRP1 and IREB2/IRP2 signals.
1068 (**H**) Quantification of Western blot signals for ACO1/IRP1 (normalised for loading via VINCULIN)
1069 from panel (G). No ACO1 is detectable in the *Aco1*$^{-/-}$ animals, as expected. ACO1 abundance is
1070 identical in the control animals at ZT5 and ZT12.
1071 (**I**) Quantification of Western blot signals for IREB2/IRP2 (normalised for loading via VINCULIN)
1072 from panel (G). IREB2 is slightly upregulated in the *Aco1*$^{-/-}$ vs. *Aco1*$^{+/+}$ animals (not significant).
1073 IREB2 levels are increased at ZT12 vs. ZT5 (** $P < 0.01$, One-way ANOVA with Šídák's multiple
1074 comparisons test).

1075 (**J**) As in (G), but for the *Ireb2*$^{-/-}$ and matched *Ireb2*$^{+/+}$ animals whose livers were used for gene
1076 expression analysis in panels (E) and (F).
1077 (**K**) Quantification of Western blot signals for ACO1/IRP1 (normalised for loading via VINCULIN)
1078 from panel (J). Differences beween timepoints or genotypes (*Ireb2*$^{-/-}$ vs. *Ireb2*$^{+/+}$) were statistically
1079 not significant (One-way ANOVA with Šídák's multiple comparisons test).
1080 (**L**) Quantification of Western blot signals for IREB2/IRP2 (normalised for loading via VINCULIN)
1081 from panel (J). IREB2 is undetectable in *Ireb2*$^{-/-}$ mice as expected. The upregulation from ZT5 to
1082 ZT12 is statistically significant (* $P < 0.05$, Student's t-test).

1083 **Figure 5. Strong timepoint- and transcript-dependence of derepression upon loss of**
1084 **ACO1/IRP1 vs. IREB2/IRP2.**
1085 (**A**) Translation efficiency analysis for *Ftl1* at ZT5 and ZT12 in the *Aco1* line (*Aco1*$^{-/-}$ vs. *Aco1*$^{+/+}$ in
1086 ochre and grey, respectively) in the left panel and for *Ireb2* line (*Ireb2*$^{-/-}$ vs. *Ireb2*$^{+/+}$ in purple and
1087 grey, respectively) in the right panel. Statistical significance evaluated by unpaired t-test and
1088 indicated with asterisks (*** $P < 0.001$, ** $P < 0.01$, * $P < 0.05$).
1089 (**B**) As in (A), for *Fth1*.
1090 (**C**) As in (A), for *Alas2*.
1091 (**D**) RPF (upper) and RNA (lower) normalised reads for *Tfrc* at ZT5 and ZT12 in the *Aco1* line
1092 (*Aco1*$^{-/-}$ vs. *Aco1*$^{+/+}$ in ochre and grey, respectively) in the left panel and for *Ireb2* line (*Ireb2*$^{-/-}$ vs.
1093 *Ireb2*$^{+/+}$ in purple and grey, respectively) in the right panel. Statistical significance evaluated by
1094 unpaired t-test and indicated with asterisks (*** $P < 0.001$, ** $P < 0.01$, * $P < 0.05$).
1095 (**E**) As in (A), for *Slc40a1*.
1096 (**F**) As in (A), for *Epas1*.
1097 (**G**) As in (A), for *Aco2*.
1098 (**H**) As in (D) for *Slc11a2/Dmt1*.
1099 (**I**) K-means clustering analysis on z-score-transformed TE profiles across all eight conditions (2
1100 timepoints, 4 genotypes; replicate means were used). The numbering of the 15 clusters and the
1101 gene count are given below the heatmap. Below the clusters, the known/validated IRE-containing
1102 transcripts are highlighted in red, with (*Tfrc* and *Slc11a2* in parantheses, given that their IRE-
1103 regulation is not at the level of TE, but of RNA stability). Predicted IRE-like mRNAs from a list in
1104 [52] are highlighted in orange. Note that the two most rhythmically translated IRE-containing
1105 mRNAs, *Ftl1* and *Fth1* are found together in cluster 8. Several other IRE transcipts are enriched
1106 in cluster 13.
1107 (**J**) Hierarchical clustering according to the similarity in TE profiles for transcripts in cluster 8 from
1108 panel (I). *Ftl1* and *Fth1* cluster together (marked in red).
1109 (**K**) Zoom into the part of cluster 8 that contains *Ftl1* and *Fth1* in direct vicinity (marked in red).
1110 The unsupervised clustering thus confirms that these two transcript indeed have a distinct mode
1111 of (rhythmic) regulation that sets them apart from other transcripts, even IRE-containing ones.
1112 (**L**) Hierarchical clustering according to the similarity in TE profiles for transcripts belonging to
1113 cluster 13 from panel (I), which contains several validated (red) and predicted (orange) IRE-
1114 containing transcripts, possibly indicating common regulatory mechanisms and, in particular,
1115 similar “set-points”.

1116 **Figure 6. Phase of *Tfrc* oscillations across feeding paradigms and clock models suggests**
1117 **that food intake is the major driver of rhythmicity in the IRP/IRE system.**
1118 (**A**) Plotting of liver *Tfrc* expression data from the study by Greco et al. [60], which included two
1119 feeding paradigms (*ad libitum* vs. night-restricted) and three genotypes (WT, full-body clock-
1120 deficient *Arntl/Bmal1* KO, liver re-expression *Arntl/Bmal1*). The upper panel indicates that night-
1121 restricted feeding exacerbates the rhythm. The middle panel shows that night-restricted feeding
1122 restores rhythmicity in an otherwise circadian clock-deficient animal. A similar outcome is seen in
1123 the *Bmal1* re-expression animals shown in the lower panel.
1124 (**B**) Analogous to (A) using the data from Atger et al. [7] that contains both mRNA and pre-mRNA
1125 reads. Thus, under night-restricted feeding, wild-type and clock-deficient *Arntl/Bmal1* knockout
1126 animals show near-identical *Tfrc* oscillations (upper panel). These oscillations are post-
1127 transcriptionally generated, given that *Tfrc* pre-mRNA levels are not rhythmic (lower panel).
1128 (**C**) Analogous to (A) and (B) using the data from Greenwell et al. [61]. The upper panel compares
1129 *ad libitum* and night-restricted feeding effect on *Tfrc*, with the latter showing higher amplitude
1130 rhythms. The lower panel shows the loss of *Tfrc* rhythms in wild-type animals (i.e., containing a
1131 functional clock) when feeding becomes gradually less rhythmic.
1132 (**D**) Analysis of dataset from Manella et al. [62] which compares wild-type animals (i.e. with a
1133 functional circadian clock) that are *ad libitum*-fed vs. exclusively day-fed. Day-feeding inverts the
1134 *Tfrc* rhythmicity.

1135 **Figures**

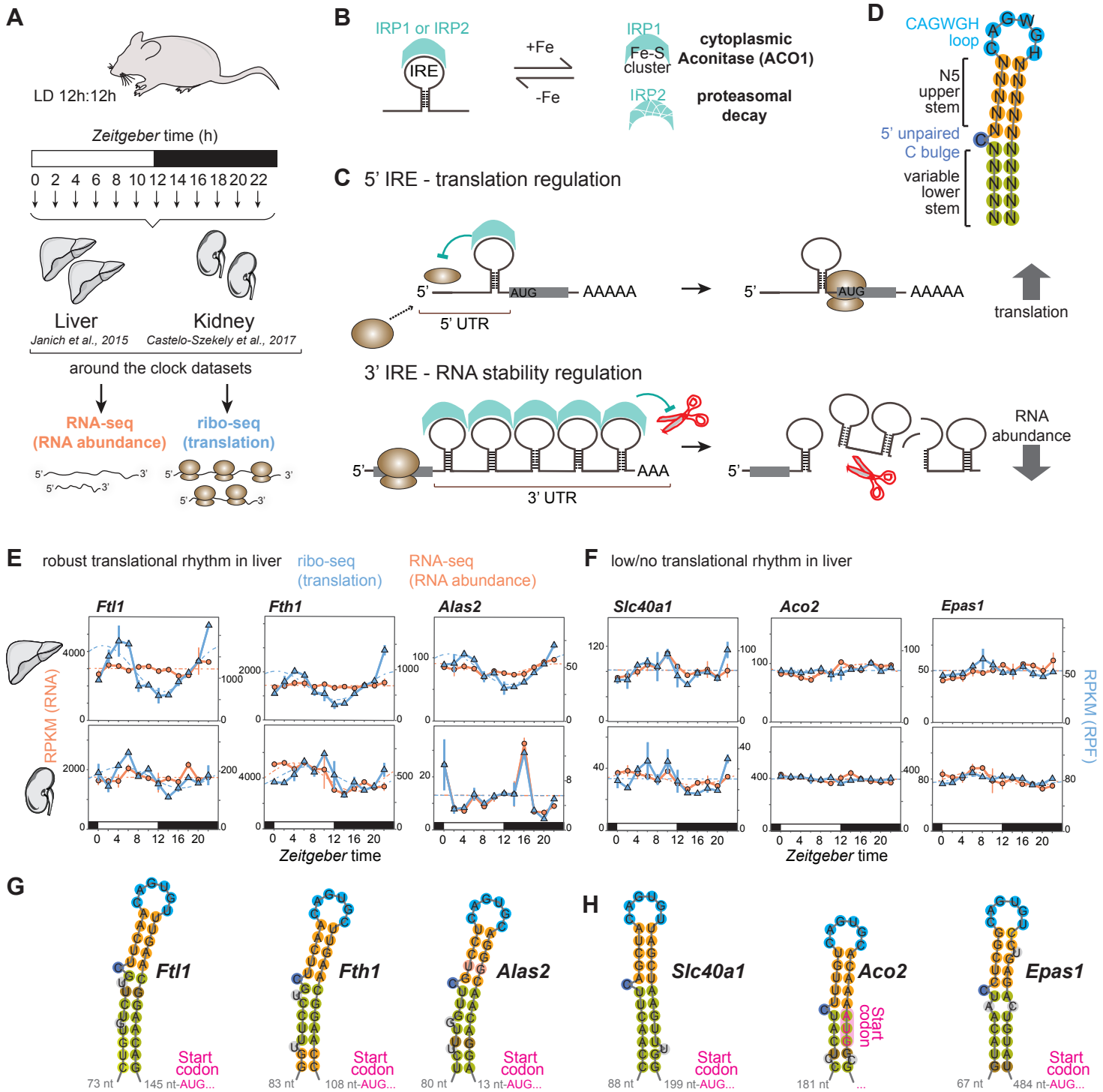
A
LD 12h:12h
Zeitgeber time (h)
0 2 4 6 8 10 12 14 16 18 20 22
Liver
Janich et al., 2015
Kidney
Castelo-Szekely et al., 2017
around the clock datasets
RNA-seq
(RNA abundance)
ribo-seq
(translation)
B
IRP1 or IRP2
IRE
+Fe
-Fe
IRP1
Fe-S
cluster
cytoplasmic
Aconitase (ACO1)
IRP2
proteasomal
decay
C 5' IRE - translation regulation
5'
AUG
AAAAA
5' UTR
translation
3' IRE - RNA stability regulation
AAA
3' UTR
RNA
abundance
D
CAGWGH
loop
N5
upper
stem
5' unpaired
C bulge
variable
lower
stem
E robust translational rhythm in liver
ribo-seq
(translation)
RNA-seq
(RNA abundance)
Ftl1
Fth1
Alas2
RPKM (RNA)
Zeitgeber time
F low/no translational rhythm in liver
Slc40a1
Aco2
Epas1
RPKM (RPF)
Zeitgeber time
G
Ftl1
Start
codon
73 nt
145 nt-AUG...
Fth1
83 nt
108 nt-AUG...
Alas2
80 nt
13 nt-AUG...
H
Slc40a1
88 nt
199 nt-AUG...
Aco2
181 nt
Start
codon
Epas1
67 nt
484 nt-AUG...

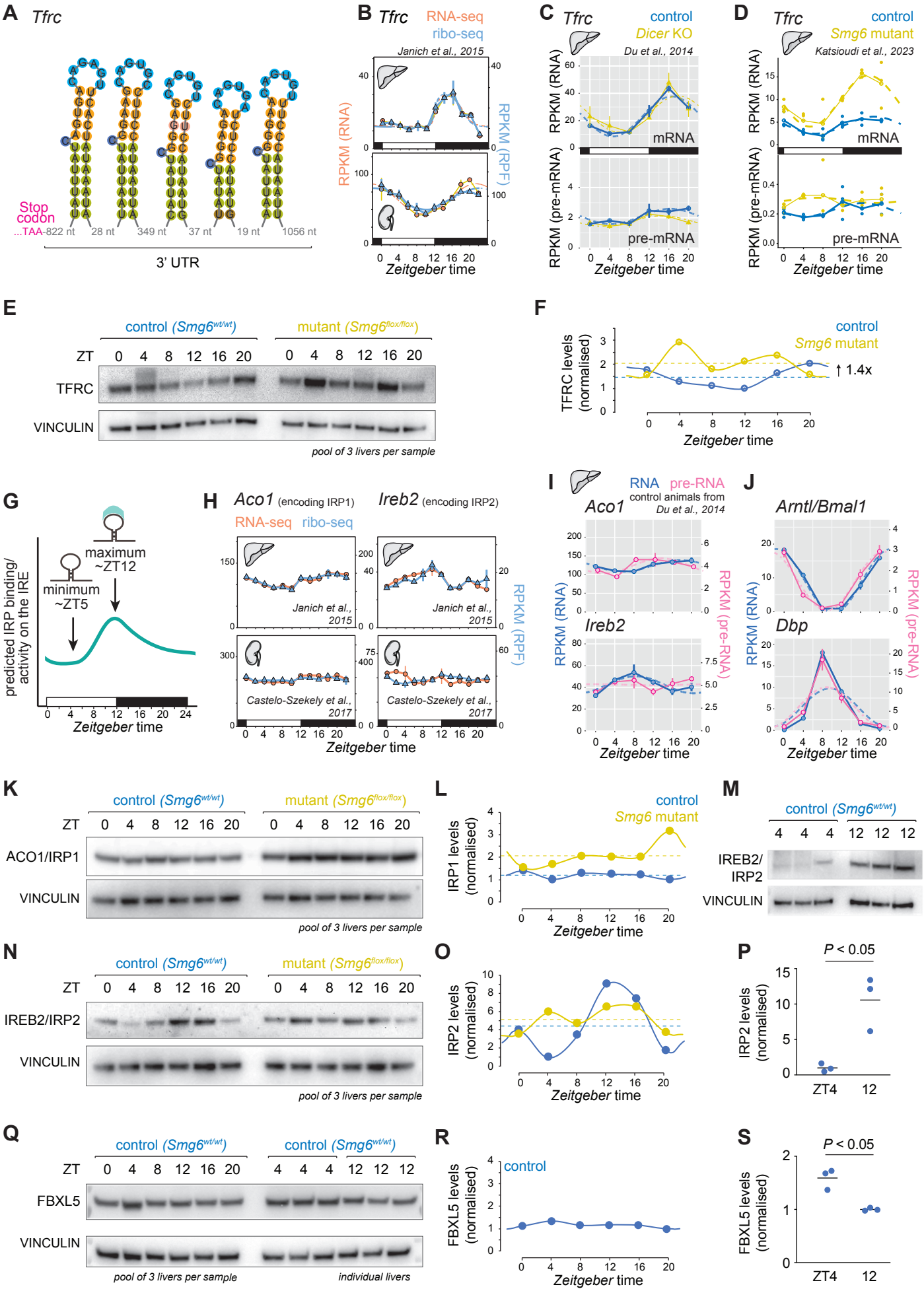
A Tfrc
Stop codon
...TAA-822 nt
28 nt
349 nt
37 nt
19 nt
1056 nt
3' UTR
B Tfrc
RNA-seq
ribo-seq
Janich et al., 2015
RPKM (RNA)
RPKM (RPF)
Zeitgeber time
C Tfrc
control
Dicer KO
Du et al., 2014
RPKM (RNA)
mRNA
RPKM (pre-mRNA)
pre-mRNA
Zeitgeber time
D Tfrc
control
Smg6 mutant
Katsioudi et al., 2023
RPKM (RNA)
mRNA
RPKM (pre-mRNA)
pre-mRNA
Zeitgeber time
E
control (Smg6wt/wt)
mutant (Smg6flox/flox)
ZT 0 4 8 12 16 20 0 4 8 12 16 20
TFRC
VINCULIN
pool of 3 livers per sample
F
control
Smg6 mutant
TFRC levels (normalised)
↑ 1.4x
Zeitgeber time
G
maximum ~ZT12
minimum ~ZT5
predicted IRP binding/ activity on the IRE
Zeitgeber time
H Aco1 (encoding IRP1)
Ireb2 (encoding IRP2)
RNA-seq
ribo-seq
Janich et al., 2015
Castelo-Szekely et al., 2017
RPKM (RPF)
Zeitgeber time
I
RNA
pre-RNA
control animals from Du et al., 2014
Aco1
Ireb2
RPKM (RNA)
RPKM (pre-RNA)
Zeitgeber time
J
Arntl/Bmal1
Dbp
RPKM (RNA)
RPKM (pre-RNA)
Zeitgeber time
K
control (Smg6wt/wt)
mutant (Smg6flox/flox)
ZT 0 4 8 12 16 20 0 4 8 12 16 20
ACO1/IRP1
VINCULIN
pool of 3 livers per sample
L
control
Smg6 mutant
IRP1 levels (normalised)
Zeitgeber time
M
control (Smg6wt/wt)
4 4 4 12 12 12
IREB2/ IRP2
VINCULIN
N
control (Smg6wt/wt)
mutant (Smg6flox/flox)
ZT 0 4 8 12 16 20 0 4 8 12 16 20
IREB2/IRP2
VINCULIN
pool of 3 livers per sample
O
IRP2 levels (normalised)
Zeitgeber time
P
P < 0.05
IRP2 levels (normalised)
ZT4
12
Q
control (Smg6wt/wt)
control (Smg6wt/wt)
ZT 0 4 8 12 16 20 4 4 4 12 12 12
FBXL5
VINCULIN
pool of 3 livers per sample
individual livers
R
control
FBXL5 levels (normalised)
Zeitgeber time
S
P < 0.05
FBXL5 levels (normalised)
ZT4
12

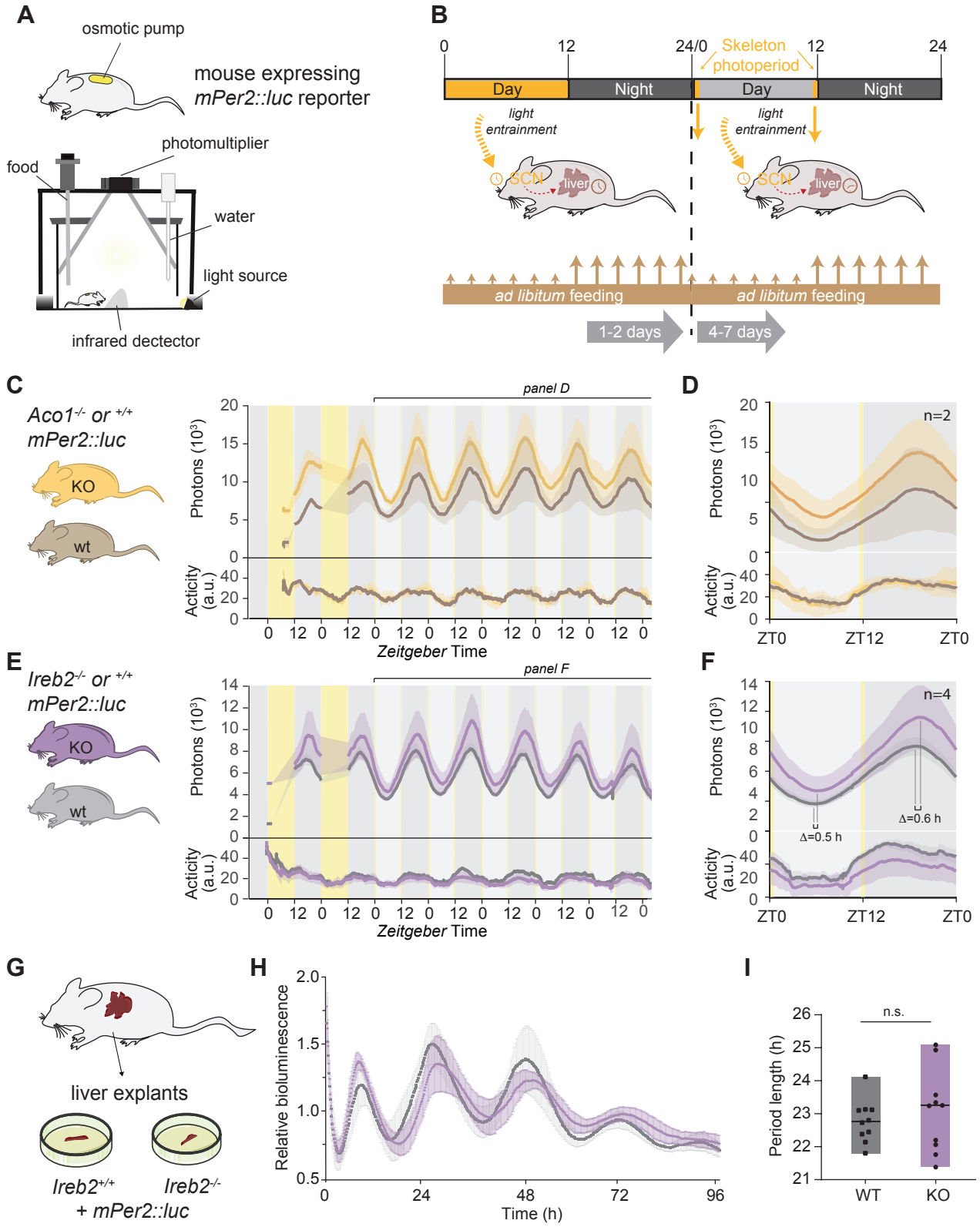
A
osmotic pump
mouse expressing
mPer2::luc reporter
photomultiplier
food
water
light source
infrared dectector
B
0
12
24/0
Skeleton photoperiod
12
24
Day
Night
Day
Night
light entrainment
light entrainment
SCN
liver
SCN
liver
ad libitum feeding
ad libitum feeding
1-2 days
4-7 days
C
Aco1-/- or +/+
mPer2::luc
KO
wt
panel D
Photons (10³)
Acticity (a.u.)
Zeitgeber Time
D
n=2
ZT0
ZT12
ZT0
E
Ireb2-/- or +/+
mPer2::luc
KO
wt
panel F
Photons (10³)
Acticity (a.u.)
Zeitgeber Time
F
n=4
Δ=0.5 h
Δ=0.6 h
ZT0
ZT12
ZT0
G
liver explants
Ireb2+/+
+ mPer2::luc
Ireb2-/-
H
Relative bioluminescence
Time (h)
I
n.s.
Period length (h)
WT
KO

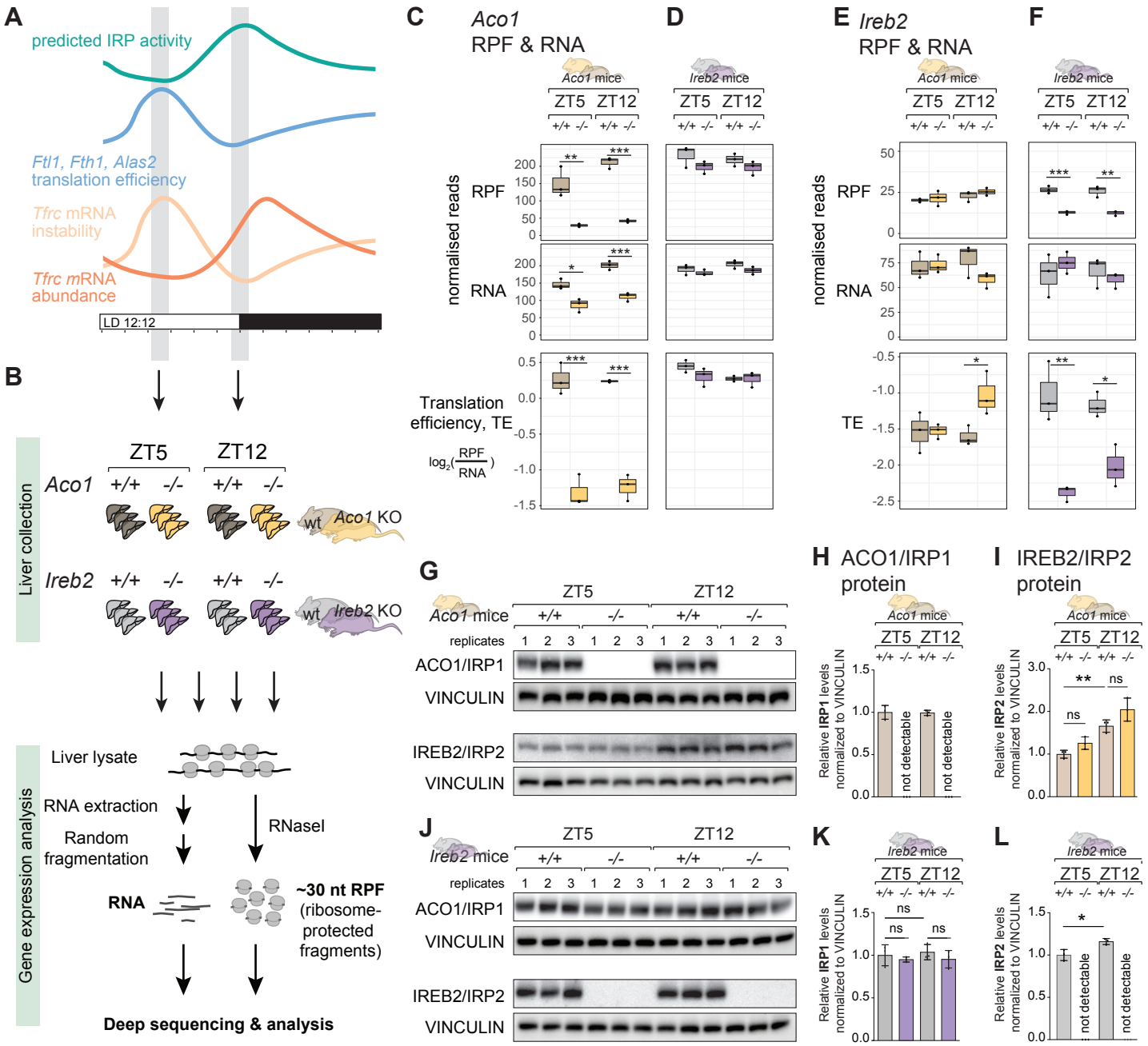
A
predicted IRP activity
Ftl1, Fth1, Alas2 translation efficiency
Tfrc mRNA instability
Tfrc mRNA abundance
LD 12:12
B
Liver collection
ZT5
ZT12
Aco1
+/+
-/-
wt
Aco1 KO
Ireb2
Ireb2 KO
Gene expression analysis
Liver lysate
RNA extraction
Random fragmentation
RNaseI
RNA
~30 nt RPF (ribosome-protected fragments)
Deep sequencing & analysis
C
Aco1 RPF & RNA
D
E
Ireb2 RPF & RNA
F
Aco1 mice
Ireb2 mice
normalised reads
RPF
RNA
Translation efficiency, TE
log2(RPF/RNA)
TE
G
Aco1 mice
replicates
ACO1/IRP1
VINCULIN
IREB2/IRP2
H
ACO1/IRP1 protein
I
IREB2/IRP2 protein
Relative IRP1 levels normalized to VINCULIN
Relative IRP2 levels normalized to VINCULIN
not detectable
ns
J
Ireb2 mice
K
L

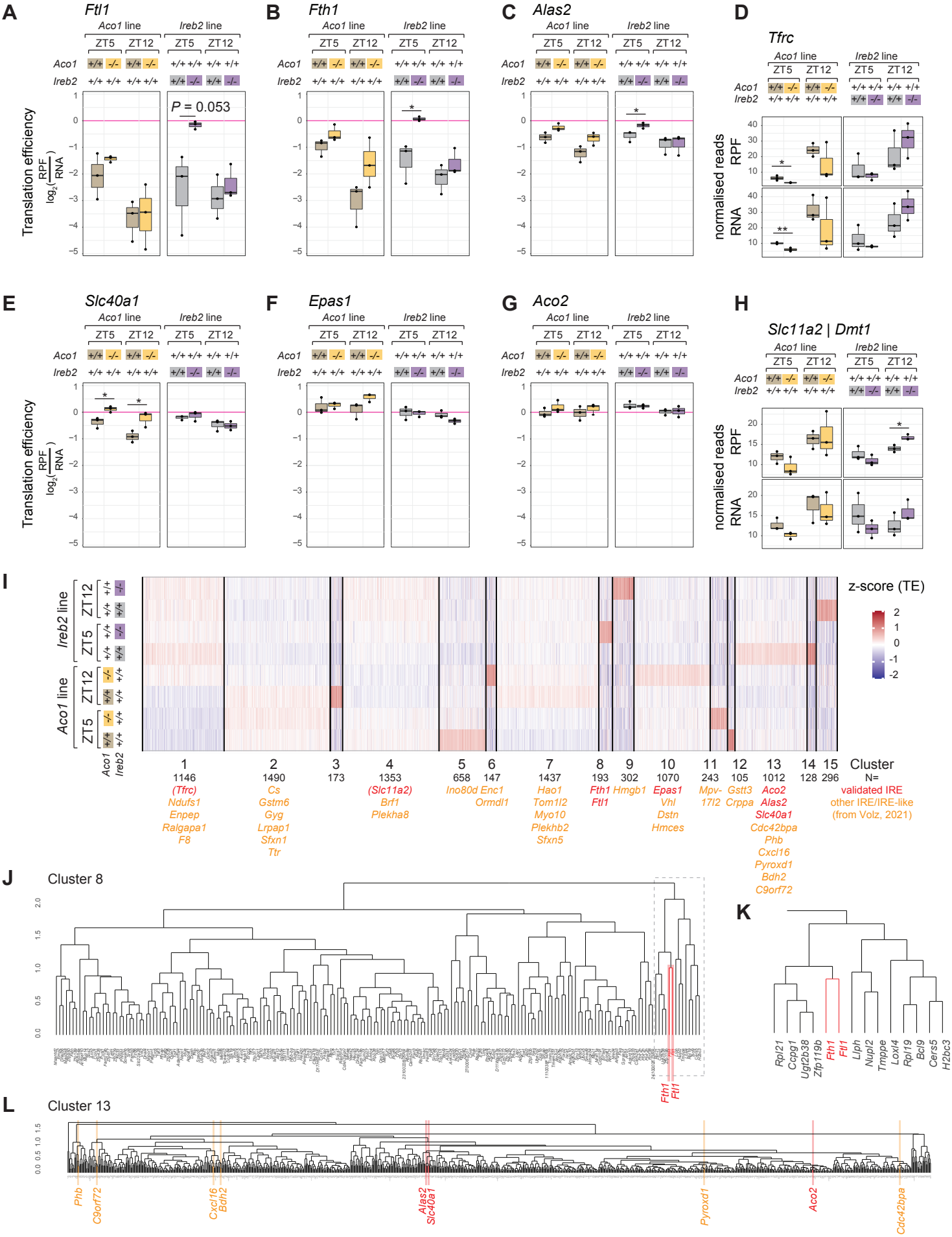
A
Ftl1
B
Fth1
C
Alas2
D
Tfrc
E
Slc40a1
F
Epas1
G
Aco2
H
Slc11a2 | Dmt1
Aco1 line
Ireb2 line
ZT5
ZT12
Aco1
Ireb2
Translation efficiency
log2(RPF/RNA)
P = 0.053
normalised reads
RPF
RNA
I
z-score (TE)
Ireb2 line
Aco1 line
Cluster
N=
validated IRE
other IRE/IRE-like
(from Volz, 2021)
1 1146 (Tfrc) Ndufs1 Enpep Ralgapa1 F8
2 1490 Cs Gstm6 Gyg Lrpap1 Sfxn1 Ttr
3 173
4 1353 (Slc11a2) Brf1 Plekha8
5 658 Ino80d
6 147 Enc1 Ormdl1
7 1437 Hao1 Tom1l2 Myo10 Plekhb2 Sfxn5
8 193 Fth1 Ftl1
9 302 Hmgb1
10 1070 Epas1 Vhl Dstn Hmces
11 243 Mpv-17l2
12 105 Gstt3 Crppa
13 1012 Aco2 Alas2 Slc40a1 Cdc42bpa Phb Cxcl16 Pyroxd1 Bdh2 C9orf72
14 128
15 296
J
Cluster 8
Fth1
Ftl1
K
Rpl21
Copg1
Ugt2b38
Zfp119b
Fth1
Ftl1
Llph
Nupl2
Tmppe
Loxl4
Rpl19
Bcl9
Cers5
H2bc3
L
Cluster 13
Phb
C9orf72
Cxcl16
Bdh2
Alas2
Slc40a1
Pyroxd1
Aco2
Cdc42bpa

**A**

Dataset:
Greco et al., Science Advances 2021
*Tfrc* RNA-seq data (mRNA)
feeding: *ad libitum* & night-restricted
mice: WT, *Bmal1* KO,
liver-specific *Bmal1* re-expression

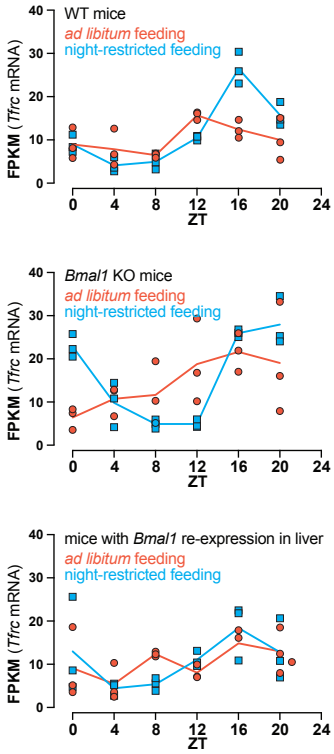


**B**

Dataset:
Atger et al., PNAS 2015
*Tfrc* RNA-seq data (mRNA & pre-mRNA)
feeding: night-restricted
mice: WT, *Bmal1* KO

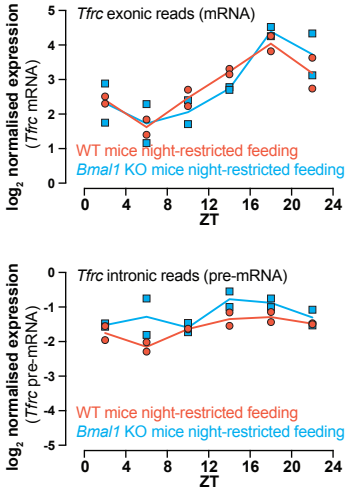


**C**

Dataset:
Greenwell et al., Cell Reports 2019
*Tfrc* RNA-seq data (mRNA)
feeding: *ad libitum*, night-restricted,
arrhythmic feeding & damped rhythm
mice: WT

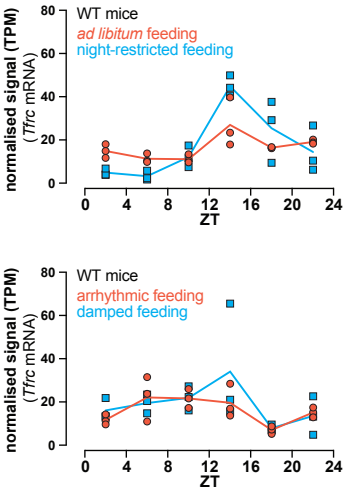


**D**
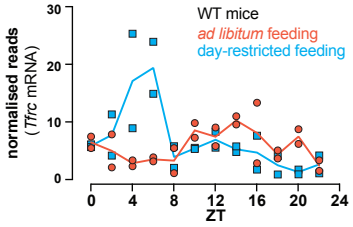
Dataset:
Manella et al., Nature Metabolism 2021
*Tfrc* RNA-seq data (mRNA )
feeding: *ad libitum* & day-restricted
mice: WT